



ELSEVIER

Contents lists available at ScienceDirect

## Journal of Computational Physics

[www.elsevier.com/locate/jcp](http://www.elsevier.com/locate/jcp)


# Compositional modeling in porous media using constant volume flash and flux computation without the need for phase identification

Ondřej Polívka, Jiří Mikyška\*

Department of Mathematics, Faculty of Nuclear Sciences and Physical Engineering, Czech Technical University in Prague, Trojanova 13, 120 00 Prague 2, Czech Republic



## ARTICLE INFO

## Article history:

Received 2 July 2013

Received in revised form 24 February 2014

Accepted 11 April 2014

Available online 24 April 2014

## Keywords:

Compositional simulation without phase identification

Mixed-hybrid finite element method

Finite volume method

Phase-by-phase upwinding

Constant-volume phase splitting

Pressure computation

## ABSTRACT

The paper deals with the numerical solution of a compositional model describing compressible two-phase flow of a mixture composed of several components in porous media with species transfer between the phases. The mathematical model is formulated by means of the extended Darcy's laws for all phases, components continuity equations, constitutive relations, and appropriate initial and boundary conditions. The splitting of components among the phases is described using a new formulation of the local thermodynamic equilibrium which uses volume, temperature, and moles as specification variables. The problem is solved numerically using a combination of the mixed-hybrid finite element method for the total flux discretization and the finite volume method for the discretization of transport equations. A new approach to numerical flux approximation is proposed, which does not require the phase identification and determination of correspondence between the phases on adjacent elements. The time discretization is carried out by the backward Euler method. The resulting large system of nonlinear algebraic equations is solved by the Newton–Raphson iterative method. We provide eight examples of different complexity to show reliability and robustness of our approach.

© 2014 Elsevier Inc. All rights reserved.

## 1. Introduction

Mathematical models of gas injection into oil reservoirs play an important role in solving problems in enhanced oil recovery or CO<sub>2</sub> sequestration. These models have to describe transport of a mixture composed of several chemical components in a porous medium. Depending on the local thermodynamic conditions, the mixture can remain in a single phase or can split into two (or more) phases. In this work, we investigate models in which components splitting among the phases is described by means of the equilibrium thermodynamics (i.e. we adopt the assumption of the local thermodynamic equilibrium).

Let us briefly review the formulation of currently available compositional models, discuss several issues inherent to this formulation, and common ways of solving these issues. Traditionally, compositional models are formulated using a set of mass or mole balance equations for each component of the mixture in which phase velocities are given by the extended version of Darcy's law [5,13,14,24]. Phases are assumed to be compressible; their behavior is described by an equation of

\* Corresponding author. Tel.: +420 224 358 553.

E-mail addresses: [ondrej.polivka@jfj.cvut.cz](mailto:ondrej.polivka@jfj.cvut.cz) (O. Polívka), [jiri.mikyška@jfj.cvut.cz](mailto:jiri.mikyška@jfj.cvut.cz) (J. Mikyška).

state, e.g. the Peng–Robinson [30] or other equation of state, of the general pressure-explicit form  $P = P(V, T, N_1, \dots, N_{n_c})$ , where  $P$  denotes the pressure,  $V$  is the volume,  $T$  is the temperature, and  $N_1, \dots, N_{n_c}$  are the mole numbers of the  $n_c$  components of the mixture. Using the assumption of the local thermodynamic equilibrium, the splitting of components between the phases is described by the equality of chemical potentials or fugacities of every component in both phases [12]. The fugacities are considered to be known functions of  $P$ ,  $T$ , and chemical composition, which can be derived from the equation of state [12,23]. Therefore, for a given specification of  $P$ ,  $T$ , and chemical composition, the stability algorithms [21, 12] can decide whether the single-phase mixture is stable or not. If the mixture is unstable,  $PT$ -flash algorithms are applied to compute the two-phase equilibrium at given  $P$  and  $T$  [22,12]. To the best of our knowledge, all available formulations of compositional models use this  $PT$ -based (constant pressure and temperature) approach to phase equilibrium computation.

No matter how wide-spread the use of the  $PT$ -based formulations of the phase stability and phase equilibria is, this approach has some limitations. First, it has been already noticed in [26,16] that specification of  $P$ ,  $T$ , and overall mole numbers (or mole fractions) does not always determine the equilibrium state of the system uniquely. For example, if we have 1 mole of pure water at  $P = 1$  atm and  $T = 100^\circ\text{C}$ , one cannot tell whether it is a saturated liquid, a saturated gas, or a two-phase mixture of both. Although all these states correspond to the same values of pressure, temperature, and moles, these states are not the same as they differ in total volume of the mixture. Note that this situation can happen in the compositional simulation if, for example, during fast injection of a pure component into a reservoir, the injected component displaces all other components from the injection cell. It is certainly desirable to have a robust model formulation which will not crash in this situation. Let us also mention that the problem of non-uniqueness of the equilibrium state at given  $P$ ,  $T$ , and  $N_1, \dots, N_{n_c}$  is not limited to pure components. We have observed the same problem in many multi-component mixtures in three phases [15].

Another complication inherent to the  $PT$ -based flash equilibrium formulations is the fact that in compositional simulation the pressure is not known a-priori. Actually, pressure field is one of the unknowns that has to be computed by the simulator. Unlike concentrations, there is no balance equation describing evolution of the pressure field. Instead, pressure is given implicitly by solving the whole system of equations. In the literature, two approaches to pressure computation in compositional simulation are available. In the first approach of Ács et al. [1], an evolution partial differential equation for pressure is formed by combining the evolution equations for overall concentrations in a suitable way. This extra equation can be solved to get the pressure field. Pressure computation is then followed by the update of concentrations using the transport equations, typically in an IMPEC (implicit pressure, explicit concentrations) manner [11,28]. As we have one more equations than unknowns, the system is overdetermined, and we have two ways to evaluate the overall concentration of the mixture – either by summing the updated overall molar concentrations of the components or by performing the  $PT$ -flash on the mixture at the predicted pressure. Due to numerical discretization errors, the two values of concentration are not the same and the mass-balance error occurs. This error can be reduced by reducing the time step. Therefore, this mass-balance error has been used as one of the criteria for the time step selection [14,34]. Let us also mention that to assemble the pressure equation, coefficients of the total two-phase compressibility and total partial molar volumes of all components have to be evaluated [12], which requires additional algebraic manipulations. An alternative approach to pressure computation is the approach of Young and Stephenson [35], in which pressure update is formed using the linearization of the transport equations with respect to selected primary variables. This approach can also be adopted in the IMPEC manner and its application also requires considerable algebraic manipulation. Moreover, the correct selection of the primary variables can be tricky as phases can appear/disappear during the simulation.

Both issues mentioned above can be overcome by using an alternative variables specification for the stability and flash equilibrium computations. By specifying volume, temperature, and moles (or temperature and overall molar concentrations of all components), the equilibrium state of the system is uniquely determined [26]. This approach requires using variables  $V$ ,  $T$ , and  $N_i$  ( $i = 1, \dots, n_c$ ) rather than the conventional set  $P$ ,  $T$ , and composition. The reformulation of the state functions like chemical potentials in terms of the new variables has been carried out in [26] and  $VT$ -based stability and flash algorithm have been derived in [26,27,16]. Within the new framework, the problem of non-uniqueness of the equilibrium state does not appear. The  $VT$ -based formulations can also be used for pressure computation because, once the temperature and overall molar concentrations are specified, equilibrium pressure is one of the outcomes of the  $VT$ -flash calculation.

In this work, we develop a new formulation of the compositional model which uses the  $VT$ -stability and  $VT$ -flash equilibrium calculation for pressure evaluation. The approach has several desirable features following from the fact that volume, temperature, and moles are the natural variables of the equation of state. In the conventional  $PT$ -flash, pressure has to be found a-priori using some of the above mentioned methods [1,35], and volume has to be computed by inverting the equation of state. The cubic equations of state may have up to three roots, from which the correct one has to be selected. Usually, the root with the lowest value of the Gibbs free energy is used [12]. In the  $VT$ -based algorithm, volume of the cell is known a-priori and pressure can be evaluated directly without the need to invert the equation of state once the resulting phase split has been computed using the  $VT$ -flash algorithm. The need for the root selection procedure is thus avoided. This feature can be even more attractive when non-cubic equation of state (like the cubic plus association equation of state) are used as in these equations number of roots is not known a-priori [18].

The approach suggested in this paper also addresses one issue not related to the  $VT$ -flash that is usually overlooked in the literature. In all formulations used for gas injection into oil reservoirs we are aware of, one usually distinguishes two phases – one of them labeled as gas and the other one labeled as liquid. In many situations of practical importance this distinction can be done easily using the phase densities, viscosities or other physical properties of the fluids. When

computing the phase fluxes across the cell boundaries, the gas phase properties on both sides of the interface are used to compute the gas phase flux across the interface between the two cells. Similarly liquid properties on both sides of the interface are used to compute the flux of the liquid phase over the interface. It is tacitly assumed that it is always possible to find out the phase identity – i.e. decide which one of the two equilibrium phases is the gas and which one is the liquid so that the correct pairing of the corresponding phases at the interface between the two grid cells is performed. This approach runs into difficulties when investigating mixtures close to the critical point where both split-phases are very similar [12]. Moreover, above the critical point, the supercritical fluids have some properties similar to liquids while other properties are similar to gases. Selection of the phase identity is then often matter of an ad-hoc procedure. It is also not clear how to compute phase fluxes between two cells with different number of phases – e.g. with one phase on one side and two phases on the other side – or between the cells which are both single-phase but one of them contains liquid and the other one gas.

Therefore, we suggest a new formulation of components fluxes in the compositional model and a special version of the upwind technique for the flux approximation which avoids the need for the phase identification. The numerical flux proposed in this work is locally conservative, does not depend on any phase identification, and solves the problem of connection of fluxes between the cells with different number of phases on both sides in a natural way. This method also helps to develop a correct formulation of the boundary conditions and avoids certain complexities encountered in our previous work [24].

The paper is structured as follows. In Section 2, the mathematical model is formulated by means of partial differential equations representing the conservation laws, Darcy's laws, and by means of the conditions of local thermodynamic equilibrium in the  $VT$ -settings. We define several fluxes and derive some relations between them. Then, the compositional model is formulated and appropriate initial and boundary conditions are prescribed. In Section 3, the system of equations is solved numerically using the Mixed-Hybrid Finite Element Method (MHFEM) for the Darcy's law discretization, and the Finite Volume Method (FVM) for the components transport equations discretization. We also describe details of the numerical flux approximation. A fully implicit scheme is derived and linearized using the Newton–Raphson iterative method (NRM). In Section 4, we summarize the essential steps of the computational algorithm. In Section 5, we present examples of computations using the new approach. In Section 6, we summarize essential features of the method and draw some conclusions. In Appendices A and B, we provide details of the equation of state used in the calculation, and details of the derivation of the MHFEM.

## 2. Mathematical model

### 2.1. Transport equations

Consider two-phase compressible flow of a mixture composed of  $n_c$  components in a porous medium with porosity  $\phi$  [–] at a constant temperature  $T$  [K]. Neglecting diffusion and capillarity, the transport of the components can be described by the following molar balance equations [24]

$$\frac{\partial(\phi c_i)}{\partial t} + \nabla \cdot \left( \sum_{\alpha} c_{\alpha,i} \mathbf{v}_{\alpha} \right) = F_i, \quad i = 1, \dots, n_c, \quad (1)$$

where  $\sum_{\alpha}$  sums over all phases,  $c_i$  is the overall molar concentration of component  $i$  [ $\text{mol m}^{-3}$ ],  $c_{\alpha,i}$  is the molar concentration of component  $i$  in phase  $\alpha$  [ $\text{mol m}^{-3}$ ], and  $F_i$  is the sink or source term [ $\text{mol m}^{-3} \text{s}^{-1}$ ]. The phase velocity  $\mathbf{v}_{\alpha}$  is given by the extended Darcy's law

$$\mathbf{v}_{\alpha} = -\lambda_{\alpha} \mathbf{K}(\nabla p - \varrho_{\alpha} \mathbf{g}), \quad \lambda_{\alpha} = \frac{k_{r\alpha}}{\mu_{\alpha}}, \quad (2)$$

where  $\mathbf{K} = \mathbf{K}(\mathbf{x})$  is the medium intrinsic permeability [ $\text{m}^2$ ],  $p$  is the pressure [Pa],  $\varrho_{\alpha} = \sum_{i=1}^{n_c} c_{\alpha,i} M_i$  is the density of fluid in phase  $\alpha$  ( $M_i$  is the molar weight of component  $i$  [ $\text{kg mol}^{-1}$ ]), and  $\mathbf{g}$  is the gravitational acceleration vector [ $\text{m s}^{-2}$ ]. The  $\alpha$ -phase mobility  $\lambda_{\alpha}$  is given by the ratio of the  $\alpha$ -phase relative permeability  $k_{r\alpha}$  [–] and  $\alpha$ -phase dynamic viscosity  $\mu_{\alpha}$  [ $\text{kg m}^{-1} \text{s}^{-1}$ ]. The  $\alpha$ -phase relative permeability depends on its saturation  $S_{\alpha}$  [–] as

$$k_{r\alpha} = k_{r\alpha}(S_{\alpha}), \quad (3)$$

and

$$\mu_{\alpha} = \mu_{\alpha}(T, c_{\alpha,1}, \dots, c_{\alpha,n_c}) \quad (4)$$

is computed using the Lohrenz–Bray–Clark method [19].

## 2.2. VT-stability and phase-split calculation

Depending on the local thermodynamic conditions at each point, the mixture can be in a single phase or split into two phases. To test whether the phase splitting occurs, we use a constant volume phase stability test described in [27]. Assuming that temperature  $T > 0$  and the overall molar concentrations  $c_1, \dots, c_{n_c}$  are known, this algorithm tests if splitting of a small amount of a trial phase with arbitrary concentrations  $c'_1, \dots, c'_{n_c}$  from the initial phase can decrease the total Helmholtz free energy of the system. If such a trial phase cannot be found, then the single phase is stable,  $c_{\alpha,i} = c_i$ ,  $S_\alpha = 1$ , and pressure is given by an equation of state of the form

$$p = p(T, c_1, \dots, c_{n_c}). \quad (5)$$

In this work, we use the Peng–Robinson equation of state, which is detailed in [Appendix A](#).

If the VT-stability indicates that the system is in two phases, the splitting of components among the phases is given by the following phase equilibrium conditions [26]

$$\sum_{\alpha} c_{\alpha,i} S_{\alpha} = c_i, \quad \sum_{\alpha} S_{\alpha} = 1, \quad (6a)$$

$$p(T, c_{\alpha,1}, \dots, c_{\alpha,n_c}) = p(T, c_{\beta,1}, \dots, c_{\beta,n_c}), \quad \forall \alpha \neq \beta, \quad (6b)$$

$$\tilde{\mu}_i(T, c_{\alpha,1}, \dots, c_{\alpha,n_c}) = \tilde{\mu}_i(T, c_{\beta,1}, \dots, c_{\beta,n_c}), \quad \forall \alpha \neq \beta, \quad \forall i = 1, \dots, n_c. \quad (6c)$$

Eqs. (6) express the balance of mass and volume (6a), mechanical equilibrium (6b), and chemical equilibrium (6c) in which  $\tilde{\mu}_i$  denotes the chemical potential of component  $i$ . Details of relations (6b) and (6c) can be found in [Appendix A](#).

The system of equations (6) represents a set of non-linear algebraic equations. If the temperature  $T$  and overall molar concentrations  $c_1, \dots, c_{n_c}$  are specified, solving (6) will provide molar concentrations of all components in both phases  $c_{\alpha,i}$  and phase saturations  $S_{\alpha}$ . Once the system (6) is resolved, the equilibrium pressure  $p$  can be determined readily using the equation of state as

$$p = p(T, c_{\alpha,1}, \dots, c_{\alpha,n_c}), \quad (7)$$

where  $\alpha$  is any of the split-phases. The value of pressure does not depend on the selection of  $\alpha$  because in equilibrium, pressures in both phases are the same, see (6b).

## 2.3. Definition of several fluxes

Let us define the  $i$ -th component flux in the  $\alpha$ -phase  $\mathbf{q}_{\alpha,i}$  and the total  $\alpha$ -phase flux  $\mathbf{q}_{\alpha}$  as

$$\mathbf{q}_{\alpha,i} = c_{\alpha,i} \mathbf{v}_{\alpha}, \quad (8a)$$

$$\mathbf{q}_{\alpha} = \sum_{i=1}^{n_c} \mathbf{q}_{\alpha,i} = c_{\alpha} \mathbf{v}_{\alpha}, \quad (8b)$$

where  $c_{\alpha} = \sum_{i=1}^{n_c} c_{\alpha,i}$  is the total  $\alpha$ -phase concentration. By summing over all phases in (8), we can calculate the total component flux  $\mathbf{q}_i$  and the total flux  $\mathbf{q}$  as

$$\mathbf{q}_i = \sum_{\alpha} \mathbf{q}_{\alpha,i} = \sum_{\alpha} c_{\alpha,i} \mathbf{v}_{\alpha}, \quad (9a)$$

$$\mathbf{q} = \sum_{\alpha} \mathbf{q}_{\alpha} = \sum_{\alpha} c_{\alpha} \mathbf{v}_{\alpha}. \quad (9b)$$

For further derivation of the numerical scheme, we need to express the phase velocity  $\mathbf{v}_{\alpha}$  using the total flux  $\mathbf{q}$ . By substituting (2) into (9b), Darcy's law for the total flux can be formulated as

$$\mathbf{q} = - \sum_{\alpha} c_{\alpha} \lambda_{\alpha} \mathbf{K} (\nabla p - \tilde{\varrho} \mathbf{g}), \quad (10)$$

where

$$\tilde{\varrho} = \frac{\sum_{\alpha} c_{\alpha} \lambda_{\alpha} \varrho_{\alpha}}{\sum_{\alpha} c_{\alpha} \lambda_{\alpha}} \quad (11)$$

is an average density. Note that although  $\lambda_{\alpha}$  can vanish when  $S_{\alpha} \rightarrow 0$ , the sum  $\sum_{\alpha} c_{\alpha} \lambda_{\alpha}$  is always positive, so the division in (11) is permissible. By inverting  $\mathbf{K}$  (which is invertible since (B.7) holds) in (10), the pressure gradient is given by

$$\nabla p = - \frac{\mathbf{K}^{-1} \mathbf{q}}{\sum_{\alpha} c_{\alpha} \lambda_{\alpha}} + \tilde{\varrho} \mathbf{g}. \quad (12)$$

Combining (12) and (2), we have

$$\mathbf{v}_\alpha = \frac{\lambda_\alpha}{\sum_\beta c_\beta \lambda_\beta} \left( \mathbf{q} - \sum_\beta c_\beta \lambda_\beta (\varrho_\beta - \varrho_\alpha) \mathbf{K} \mathbf{g} \right). \quad (13)$$

Then, using (8a) and (13),  $\mathbf{q}_{\alpha,i}$  can be evaluated as

$$\mathbf{q}_{\alpha,i} = \frac{c_{\alpha,i} \lambda_\alpha}{\sum_\beta c_\beta \lambda_\beta} \left( \mathbf{q} - \sum_\beta c_\beta \lambda_\beta (\varrho_\beta - \varrho_\alpha) \mathbf{K} \mathbf{g} \right), \quad (14)$$

and the total component flux (combining (9a) and (13)) as

$$\mathbf{q}_i = \sum_\alpha \frac{c_{\alpha,i} \lambda_\alpha}{\sum_\beta c_\beta \lambda_\beta} \left( \mathbf{q} - \sum_\beta c_\beta \lambda_\beta (\varrho_\beta - \varrho_\alpha) \mathbf{K} \mathbf{g} \right). \quad (15)$$

#### 2.4. Model formulation

Let  $\Omega \subset \mathbb{R}^d$  ( $d \in \mathbb{N}$ ) be a bounded domain and  $I$  be a time interval. In  $\Omega \times I$ , we solve for  $c_i = c_i(\mathbf{x}, t)$  the following equations which can be obtained from the transport equations (1) and (9a)

$$\frac{\partial(\phi c_i)}{\partial t} + \nabla \cdot \mathbf{q}_i = F_i, \quad i = 1, \dots, n_c, \quad (16)$$

where  $\mathbf{q}_i$  is given by (15), and  $\mathbf{q}$  is given by (10). The molar concentrations  $c_{\alpha,i}$  and saturations  $S_\alpha$  are related to the overall molar concentrations  $c_i$  by (6) from which we also determine the pressure (see Section 2.2). Relative permeabilities and viscosities are given by (3) and (4). For this system of equations, we impose the following initial and boundary conditions

$$c_i(\mathbf{x}, 0) = c_i^0(\mathbf{x}), \quad \mathbf{x} \in \Omega, \quad i = 1, \dots, n_c, \quad (17a)$$

$$p(\mathbf{x}, t) = p^D(\mathbf{x}, t), \quad \mathbf{x} \in \Gamma_p, \quad t \in I, \quad (17b)$$

$$\mathbf{q}_i(\mathbf{x}, t) \cdot \mathbf{n}(\mathbf{x}) = 0, \quad \mathbf{x} \in \Gamma_q, \quad t \in I, \quad i = 1, \dots, n_c, \quad (17c)$$

where  $\mathbf{n}$  is the unit outward normal vector to the boundary  $\partial\Omega$ ,  $\Gamma_p \cup \Gamma_q = \partial\Omega$ , and  $\Gamma_p \cap \Gamma_q = \emptyset$ . Initial values of molar concentrations are given by (17a), whereas (17b) is the Dirichlet boundary condition prescribing the pressure  $p_D$  on  $\Gamma_p$ , and (17c) is zero Neumann boundary condition representing impermeable boundary on  $\Gamma_q$ . We assume that  $\Gamma_p$  is the outflow boundary, so no boundary condition for concentration has to be imposed.

### 3. Numerical scheme

The system of equations (16), (6), and (17) is solved numerically by a combination of the MHFEM for the total flux discretization, and the FVM for the transport equations discretization. The system is linearized using the NRM. The local number of phases on every element is determined by testing the single-phase stability at constant temperature and overall molar concentrations using the constant volume stability algorithm described in [27]. In two-phase elements, the splitting of components among the phases is computed using the VT-flash algorithm from [26]. Once the phase state (i.e. single-phase or two-phase) of every element and the phase splitting in two-phase elements have been established, pressure is computed explicitly using the equation of state.

We consider a 2D polygonal domain  $\Omega$  with the boundary  $\partial\Omega$  which is covered by a conforming triangulation  $\mathcal{T}_\Omega$ . Let us denote  $K$  the element of the mesh  $\mathcal{T}_\Omega$  with area  $|K|$ ,  $E$  the edge of an element with the length  $|E|$ ,  $n_k$  the number of elements of the triangulation, and  $n_e$  the number of edges of the mesh.

#### 3.1. Discretization of the total flux

The total flux  $\mathbf{q}$  is approximated locally in the Raviart–Thomas space of the lowest order ( $\text{RT}_0(K)$ ) over the element  $K \in \mathcal{T}_\Omega$  [3] as

$$\mathbf{q}|_K = \sum_{E \in \partial K} q_{K,E} \mathbf{w}_{K,E}, \quad (18)$$

where the coefficient  $q_{K,E}$  is the numerical flux of vector function  $\mathbf{q}$  through the edge  $E$  on the element  $K$  with respect to the outer normal, and  $\mathbf{w}_{K,E}$  represents the piecewise linear  $\text{RT}_0(K)$ -basis function associated with the edge  $E$  (see Appendix B).

Multiplying relation (12) by the basis function  $\mathbf{w}_{K,E}$ , integrating over the element  $K$ , and using the  $RT_0(K)$  properties described in details in Appendix B, we obtain a discrete form of Darcy’s law for the total flux (10) as follows

$$q_{K,E} = \sum_{\alpha \in \Pi(K)} c_{\alpha,K} \lambda_{\alpha,K} \left( \alpha_E^K p_K - \sum_{E' \in \partial K} \beta_{E,E'}^K \widehat{p}_{K,E'} + \gamma_E^K \widetilde{Q}_K \right), \quad E \in \partial K. \tag{19}$$

In Eq. (19),  $\Pi(K)$  denotes all phases on element  $K$ . The coefficients  $\alpha_E^K$ ,  $\beta_{E,E'}^K$  and  $\gamma_E^K$  dependent on the mesh geometry and on the local values of the medium permeability are detailed in Appendix B. Further,  $p_K$  denotes the cell pressure average,  $\widehat{p}_{K,E'}$  is the edge pressure average,  $c_{\alpha,K}$ ,  $\lambda_{\alpha,K}$ ,  $\widetilde{Q}_K$  are the mean values of concentration and mobility of phase  $\alpha$ , and average density on element  $K$ . The cell-averaged quantities are functions of the overall molar concentrations and temperature at element  $K$ ; their evaluation is described in Section 3.3.

The continuity of normal component of the total flux and pressure on the edge  $E$  between neighboring elements  $K, K' \in \mathcal{T}_\Omega$  can be written as

$$q_{K,E} + q_{K',E} = 0, \tag{20}$$

$$\widehat{p}_{K,E} = \widehat{p}_{K',E} =: \widehat{p}_E. \tag{21}$$

The boundary conditions (17b), (17c) are discretized as

$$\widehat{p}_E = p^D(E), \quad \forall E \subset \Gamma_p, \tag{22a}$$

$$q_{K,E} = 0, \quad \forall E, K : E \subset \Gamma_q, E \in \partial K, \tag{22b}$$

where  $p^D(E)$  is the prescribed value of pressure  $p$  averaged on the edge  $E$ .

The numerical flux can be eliminated by substituting  $q_{K,E}$  from (19) into (20) and (22b). For further derivation, let us consider time dependent quantities at time  $t_{n+1}$  denoted by upper index  $n + 1$ . Then, Eqs. (19)–(22) can be transformed to the following system of  $n_e$  linear algebraic equations  $\mathcal{F}_E = 0$ , where

$$\mathcal{F}_E = \begin{cases} \sum_{K: E \in \partial K} \left( \sum_{\alpha \in \Pi(K)} c_{\alpha,K}^{n+1} \lambda_{\alpha,K}^{n+1} \right) (\alpha_E^K p_K^{n+1} - \sum_{E' \in \partial K} \beta_{E,E'}^K \widehat{p}_{E'}^{n+1} + \gamma_E^K \widetilde{Q}_K^{n+1}), & \forall E \notin \Gamma_p, \\ \widehat{p}_E^{n+1} - p^D(E), & \forall E \subset \Gamma_p. \end{cases} \tag{23}$$

Herein, the symbol  $\sum_{K: E \in \partial K}$  denotes the sum over the elements adjacent to the edge  $E$ .

### 3.2. Approximation of the transport equations

The transport equations (16) with the initial and boundary conditions (17) are discretized by the FVM [17]. Integrating (16) over an arbitrary element  $K \in \mathcal{T}_\Omega$  and using Green’s theorem, we have

$$\frac{d}{dt} \int_K \phi(\mathbf{x}) c_i(\mathbf{x}, t) + \int_{\partial K} \mathbf{q}_i(\mathbf{x}, t) \cdot \mathbf{n}_{\partial K}(\mathbf{x}) = \int_K F_i(\mathbf{x}), \quad i = 1, \dots, n_c. \tag{24}$$

Applying the mean value theorem on (24), and denoting  $\phi_K, c_{i,K}, F_{i,K}$ , the averaged values of  $\phi, c_i, F_i$  ( $i = 1, \dots, n_c$ ) over the cell  $K$ , respectively, the semi-discrete form of (16) reads as

$$\frac{d(\phi_K c_{i,K})}{dt} |K| + \sum_{E \in \partial K} q_{i,K,E} = F_{i,K} |K|, \tag{25}$$

where  $q_{i,K,E}$  is a numerical approximation of  $\int_E \mathbf{q}_i \cdot \mathbf{n}_{K,E}$  for  $E \in \partial K$ . The numerical flux  $q_{i,K,E}$  is evaluated by the following upwind technique

$$q_{i,K,E} = \begin{cases} \sum_{\alpha \in \Pi(K,E)^+} q_{\alpha,i,K,E} - \sum_{\beta \in \Pi(K',E)^+} q_{\beta,i,K',E}, & \forall E \notin \partial \Omega, \\ \sum_{\alpha \in \Pi(K,E)^+} q_{\alpha,i,K,E}, & \forall E \in \Gamma_p, \\ 0, & \forall E \in \Gamma_q, \end{cases} \tag{26}$$

where  $\Pi(K, E)^+ = \{\alpha \in \Pi(K) \mid q_{\alpha,i,K,E} > 0\}$  for  $E \in \partial K$ , and  $q_{\alpha,i,K,E}$  is (14) written in a discrete form as

$$q_{\alpha,i,K,E} = \frac{c_{\alpha,i,K} \lambda_{\alpha,K}}{\sum_{\beta \in \Pi(K)} c_{\beta,K} \lambda_{\beta,K}} \left( q_{K,E} - \sum_{\beta \in \Pi(K)} c_{\beta,K} \lambda_{\beta,K} (Q_{\beta,K} - Q_{\alpha,K}) \gamma_E^K \right). \tag{27}$$

Notice that (26) is an approximation of (15), where we sum over the phases on the edge  $E$  taking only the outflowing phases into account. This method ensures that no phase identification or phase interconnection between neighboring elements is necessary, and the total component fluxes are balanced on each inner edge. In (27),  $q_{K,E}$  is given by (19),  $c_{\alpha,i,K}$

and  $S_{\alpha,K}$  are computed locally on each element by  $VT$ -flash (see Section 2.2), and from them,  $c_{\alpha,K}$ ,  $\lambda_{\alpha,K}$ , and  $Q_{\alpha,K}$  are evaluated.

Assuming that the porosity does not depend on time, the time derivative of  $c_{i,K}$  in (25) is approximated by the time difference with a time step  $\Delta t_n$ . Using Euler's method [17], we obtain for every  $n$ , all  $K \in \mathcal{T}_\Omega$ , and  $i = 1, \dots, n_c$  Eq. (25) in a form  $\mathcal{F}_{K,i} = 0$ , where

$$\mathcal{F}_{K,i} = \phi_K |K| \frac{c_{i,K}^{n+1} - c_{i,K}^n}{\Delta t_n} + \sum_{E \in \partial K} q_{i,K,E}^{n+1} - F_{i,K} |K|, \tag{28}$$

where  $q_{i,K,E}$  is given by (26). Note that scheme (28) is fully implicit.

The initial conditions (17a) are approximated as

$$c_{i,K}^0 = c_i^0(K), \quad \forall K \in \mathcal{T}_\Omega, \quad i = 1, \dots, n_c, \tag{29}$$

where  $c_i^0(K)$  denotes the average value of  $c_i^0$  on element  $K$ .

### 3.3. Assembling the final scheme

In Eqs. (23) and (28), we have denoted  $\mathcal{F}_E$  and  $\mathcal{F}_{K,i}$ , (for the edge  $E \in \{1, \dots, n_e\}$ , element  $K \in \{1, \dots, n_k\}$ , and component  $i \in \{1, \dots, n_c\}$ ) the expressions which represent the components of a vector  $\mathcal{F}$ . To evaluate coefficients  $c_{\alpha,K}^{n+1}$ ,  $\lambda_{\alpha,K}^{n+1}$ ,  $\tilde{Q}_K^{n+1}$  that are needed in (23) and also other element-averaged quantities depending on phase splitting required in (26)–(28), we perform the  $VT$ -flash calculation on element  $K$  using the cell-averaged values  $c_{1,K}^{n+1}, \dots, c_{n_c,K}^{n+1}$ , and temperature  $T$ . The cell average pressure  $p_K^{n+1}$  is also given implicitly by the result of the  $VT$ -flash at given  $c_{1,K}^{n+1}, \dots, c_{n_c,K}^{n+1}$ , and temperature  $T$  as described in Section 2.2. Using the NRM, we therefore solve a nonlinear system of algebraic equations of  $n_k \cdot n_c + n_e$  equations

$$\mathcal{F} = [\mathcal{F}_{1,1}, \dots, \mathcal{F}_{1,n_c}, \dots, \mathcal{F}_{n_k,1}, \dots, \mathcal{F}_{n_k,n_c}; \mathcal{F}_1, \dots, \mathcal{F}_{n_e}]^T = \mathbf{0} \tag{30}$$

for unknown primary variables – overall molar concentrations  $c_{1,K}^{n+1}, \dots, c_{n_c,K}^{n+1}$ ,  $K \in \{1, \dots, n_k\}$ , and pressures on edges  $\hat{p}_E^{n+1}$ ,  $E \in \{1, \dots, n_e\}$ . In each iteration of the NRM, we solve the following linear system of algebraic equations

$$\mathbf{J}\delta = -\mathcal{F}. \tag{31}$$

The Jacobian matrix  $\mathbf{J}$  of system (31) is sparse and nonsymmetric. The matrix is divided into 4 blocks whose elements can be evaluated analytically using the following relations

$$(\mathbf{J}_{K,K'})_{i,j} = \frac{\partial \mathcal{F}_{K,i}}{\partial c_{j,K'}^{n+1}}, \quad (\mathbf{J}_{K,E})_i = \frac{\partial \mathcal{F}_{K,i}}{\partial \hat{p}_E^{n+1}}, \quad (\mathbf{J}_{E,K})_j = \frac{\partial \mathcal{F}_E}{\partial c_{j,K}^{n+1}}, \quad J_{E,E'} = \frac{\partial \mathcal{F}_E}{\partial \hat{p}_{E'}^{n+1}}, \tag{32}$$

where  $J_{E,E'}$  is an element of the matrix  $\mathbf{J}_{E,E'}$ ,  $i, j = 1, \dots, n_c$ ;  $K, K' = 1, \dots, n_k$ ;  $E, E' = 1, \dots, n_e$ . The vector of solutions  $\delta$  contains the corrections of molar concentrations  $\delta c_{i,K}^{n+1}$  and pressures on the edges  $\delta \hat{p}_E^{n+1}$ , which are computed in each NRM iteration and added to the values of  $c_{i,K}^{n+1}$  and  $\hat{p}_E^{n+1}$  given from the previous iteration. The iteration procedure ends when the condition

$$\|\mathcal{F}\| < \varepsilon \tag{33}$$

is satisfied for a chosen  $\varepsilon > 0$  [33]. The robustness of the NRM is increased by using the line-search technique [33]. If the NRM cannot converge in 10 iterations or if the line-search does not lead to the reduction of  $\|\mathcal{F}\|$  in 10 iterations, the time step is restarted and the value  $\Delta t_n$  is halved. If the NRM converges in less than 4 iterations, the time step is accepted and the next time step size is increased ( $\Delta t_{n+1} = 1.2\Delta t_n$ ).

Let us point out that the linearization is performed with respect to the overall molar concentrations on each element and traces of pressure on every edge of the triangulation. These variables are persistent – i.e. well defined independently of whether a given element is in a single phase or two phases. The derivatives in (32) are also well defined in both single phase and two phases. Therefore, our scheme performs well in both cases and no primary variables switching is needed for treating phase appearance/disappearance (cf. [2,6,29]). As the discretization of the transport equations is based on the approximation of the total component flux, the connection between the elements with different number of phases is treated in a natural way.

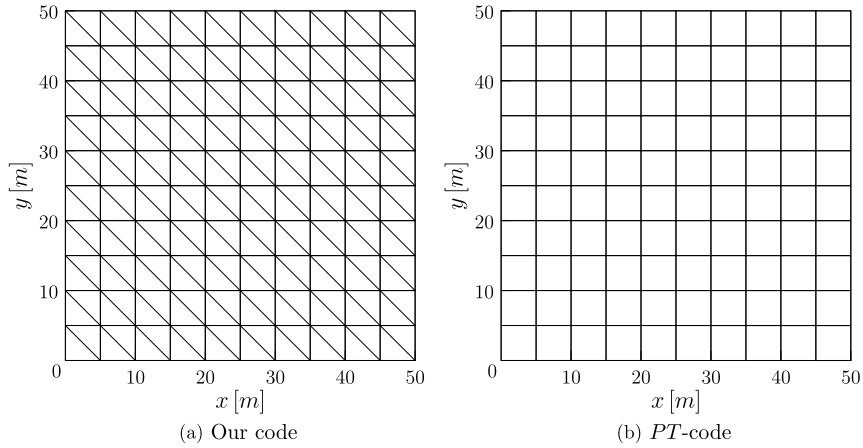


Fig. 1. Structures of the computational grid in our code and *PT*-code.

#### 4. Computational algorithm

Numerical solution can be computed in the following steps:

1. Initialize the geometry, physical and chemical parameters, and molar concentrations, generate a domain triangulation.
2. Calculate pressures  $p_K$  on each element using the equation of state (A.1) and initial molar concentrations, then initialize all edge pressures  $\hat{p}_E$  by averaging  $p_K$  on neighboring elements.
3. Repeat until the predetermined final time is reached ( $t_n \in I$ ):
  - (a) Repeat the NRM iterations until the convergence criterion (33) is satisfied:
    - i. Perform the stability and flash calculations (see Section 2.2) to obtain a number of phases and their compositions locally on all elements.
    - ii. Evaluate phase mobilities  $\lambda_{\alpha,K}^{n+1}$  using (2), (3), and (4) on each element.
    - iii. For each  $K$ , compute the cell-averaged pressures  $p_K^{n+1}$  using (5) or (6b) depending on the phase state (see Section 2.2), and average densities  $\tilde{\rho}_K^{n+1}$  using (11).
    - iv. Evaluate the total fluxes  $q_{K,E}^{n+1}$  using (19) and phase fluxes  $q_{\alpha,i,K,E}^{n+1}$  using (27).
    - v. Assemble and solve the system (31) for corrections of molar concentrations  $\delta c_{i,K}^{n+1}$  and pressures  $\delta \hat{p}_E^{n+1}$  simultaneously.
    - vi. Add corrections  $\delta c_{i,K}^{n+1}$  and  $\delta \hat{p}_E^{n+1}$  to  $c_{i,K}^{n+1}$  and  $\hat{p}_E^{n+1}$ , respectively, check the convergence criterion (33).
  - (b) Continue to the next time level ( $n \rightarrow n + 1$ ).

In steps i.–iii.  $c_{\alpha,K}^{n+1}$ ,  $\lambda_{\alpha,K}^{n+1}$ ,  $\tilde{\rho}_K^{n+1}$ , and  $p_K^{n+1}$  are computed using the data from the last available Newton iteration. In the first iteration, data from the previous time step are used.

#### 5. Numerical results

In this section, we present results of compositional simulations of gas injections into reservoirs filled with different mixtures using the numerical scheme described above. We compute the flow in a 2D square reservoir  $50 \times 50 \text{ m}^2$  with porosity  $\phi = 0.2$  and isotropic permeability  $\mathbf{K} = k = 9.87 \times 10^{-15} \text{ m}^2$  (i.e. 10 mD) if not specified otherwise. Structure of the computational grid with  $2 \times 10 \times 10$  elements is shown in Fig. 1(a). Parameter  $\varepsilon$  from the NRM convergence criterion (33) was chosen  $10^{-6}$  for all computations. The systems of linear algebraic equations were solved using the direct solver UMFPACK [7–10]. All our results were computed on a grid of  $2 \times 40 \times 40$  elements except for the simulations serving for the convergence verification. Our calculations were performed on Six-Core AMD Opteron(tm) Processor 2427 at 2.2 GHz and 32 GB memory. Only *VT*-flash calculations were performed in parallel. The rest of the computation was sequential.

In the following parts, the numerical simulations are computed for different mixtures, and validated with results computed using an other code. The other code uses the method of Ács et al. [1] to decouple pressure computation and the update of concentrations. While the pressure equation is treated semi implicitly using the MHFEM, the update of concentrations is performed explicitly using the first order FVM upwind scheme. The phase splitting is solved using the conventional *PT*-flash, and the phase identification is performed using the densities of the split phases. Details of the scheme can be found in [13,14,24]. In the following, we denote this code as *PT*-code. Note that in [24] a higher order scheme is used for computations. In this paper, we compare our results with those obtained by the first order (MHFEM–FVM) variant of the scheme [24] on a rectangular grid with structure shown in Fig. 1(b). Examples 1 and 2 correspond to Examples 3 and 4

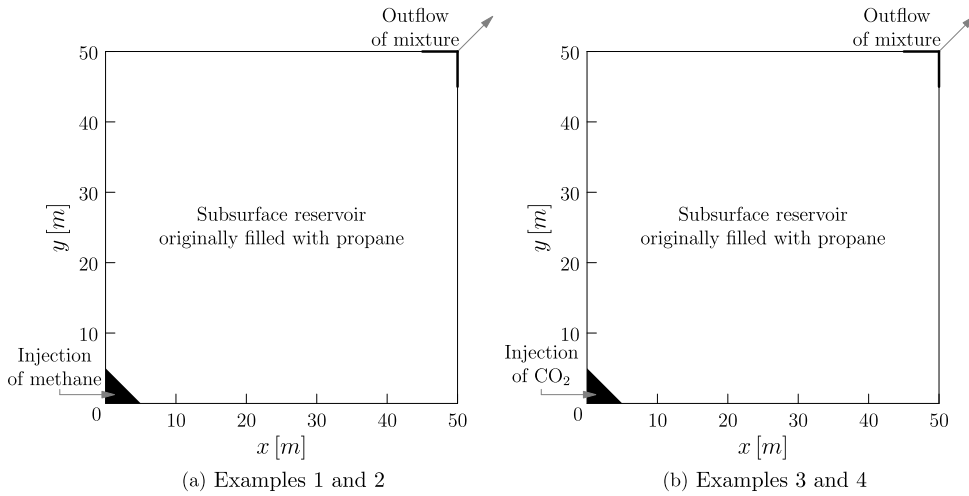


Fig. 2. Outlines of the simulated reservoirs for Examples 1–4.

Table 1

Relevant parameters of the Peng–Robinson equation of state (A.1) for Examples 1 and 2. Volume translation is not used.

$i$ (component)	$p_{ci}$ [MPa]	$T_{ci}$ [K]	$V_{ci}$ [ $\text{m}^3 \text{mol}^{-1}$ ]	$M_i$ [g mol $^{-1}$ ]	$\omega_i$ [-]	$\delta_{i1}$ [-]	$\delta_{i2}$ [-]
1 (C <sub>1</sub> )	4.58373	189.743	$9.897054 \times 10^{-5}$	16.2077	$1.14272 \times 10^{-2}$	0	0.0365
2 (C <sub>3</sub> )	4.248	369.83	$2 \times 10^{-4}$	44.0962	0.153	0.0365	0

in [24]. Examples 3 and 4 are inspired by Example 2 in [25]. Examples 6 and 7 correspond to Examples 6 and 5 in [24]. Example 8 demonstrates a case in which the traditional  $PT$ -based approach fails.

### 5.1. Injection of methane into propane

Let us consider a cut through a propane reservoir at initial pressure  $p = 6.9$  MPa and temperature  $T = 311$  K. In the left bottom corner of the reservoir, methane is injected, and in the right upper corner, the mixture of methane and propane is produced (Fig. 2(a)). The injection rate of methane is  $42.5 \text{ m}^2/\text{day}$  at pressure 1 atm (0.101325 MPa) and temperature 293 K. The parameters of the Peng–Robinson equation of state for both components of the mixture are summarized in Table 1. In these settings, both methane and propane are single-phase but when mixed, the mixture can split into two phases. The boundary of the domain is impermeable except for the outflow corner where pressure  $p = 6.9$  MPa is maintained. Relative permeability depends linearly on saturation as  $k_{r\alpha}(S_\alpha) = S_\alpha$  for each phase  $\alpha$ .

**Example 1.** First, we simulate injection of methane into a horizontal reservoir (i.e. with zero gravity) originally filled with propane. Isolines of methane overall molar fraction  $c_1/(\sum_{i=1}^2 c_i)$  at three different times are shown in Fig. 3. The value of molar fraction nearest to the injection corner is 0.95, and with each isoline towards the outflow corner the value decreases by 0.1. The mixture stays in the single phase in the major part of the domain, but, in the mixing zone, the two-phase region develops (visualized by gray color). The computation to  $t = 1.71$  years lasted 13.1 hours. To validate our results, the problem was computed also by the  $PT$ -code. The obtained result at  $t = 1.14$  years is depicted in Fig. 3(d) (indication of the two-phase region was unavailable in the  $PT$ -code). The result is similar to the one in Fig. 3(b).

In this example, we also verify convergence of the numerical scheme. In the single-phase case, an analytical solution for a special problem is available. The experimental convergence analysis of the MHFEM–FVM for this problem can be found in [32]. As, to the best of our knowledge, there is no analytical solution for the two-phase case available, we use a pseudoanalytical solution, i.e. the numerical solution computed on the finest grid of 8192 elements, for the convergence analysis. Experimental orders of convergence (EOC) are computed between neighboring grids  $m = 2 \times 2 \times 2$ ,  $2 \times 4 \times 4$ ,  $2 \times 8 \times 8$ ,  $2 \times 16 \times 16$ , and  $2 \times 32 \times 32$  using the  $L^1$  and  $L^2$  consistent norms for errors  $E_m$  of methane concentrations and cell-averaged pressures in comparison with the solution obtained on the grid  $2 \times 64 \times 64$ . The errors are computed on the finest grid by projecting the solutions from the coarser grids to the finest grid. The time step for the pseudoanalytical solution is chosen constant  $\Delta t = 195.3125$  s. For the solutions on coarser grids,  $\Delta t$  is 4 times larger with each mesh refinement ( $\Delta t \sim m^{-1}$ ), i.e.  $\Delta t = 781.25$  s for the solution computed on 2048 elements,  $\Delta t = 3125$  s for 512 elements,  $\Delta t = 12500$  s for 128 elements,  $\Delta t = 50000$  s for 32 elements, and  $\Delta t = 200000$  s for 8 elements. The EOC in a norm  $\|\cdot\|_V$  is given by

$$\text{EOC}_V = \frac{\ln \|E_{m_1}\|_V - \ln \|E_{m_2}\|_V}{\ln m_2 - \ln m_1},$$

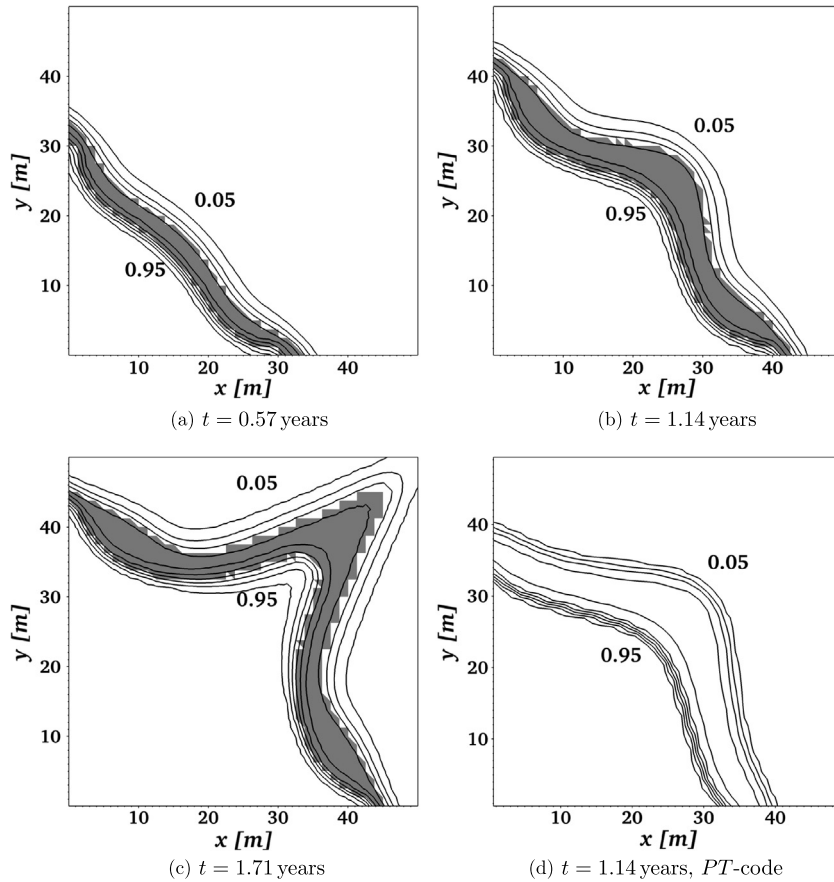


**Fig. 3.** Isolines of methane overall molar fraction and the two-phase region (gray color) at different times. Contours are distributed uniformly between the two printed values. The solution is computed on the triangular grid  $2 \times 40 \times 40$ ; (d) is computed on  $40 \times 40$  rectangles using the *PT*-code (the two-phase region is not indicated here); [Example 1](#).

**Table 2**

Experimental orders of convergence and errors of methane concentration  $c_1$  at time  $t = 0.48$  years for grids of  $m$  elements compared with the numerical solution on the grid of 8192 elements and the time step  $\Delta t = 195.3125$  s. On coarser grids,  $\Delta t \sim m^{-1}$ .

$m$	$\ E_m\ _1$	$EOC_1$	$\ E_m\ _2$	$EOC_2$
8	$7.3988 \times 10^5$		$3.3186 \times 10^4$	
32	$5.3833 \times 10^5$	0.4588	$2.7844 \times 10^4$	0.2532
128	$3.3342 \times 10^5$	0.6912	$1.8615 \times 10^4$	0.5809
512	$2.5125 \times 10^5$	0.4082	$1.7232 \times 10^4$	0.1114
2048	$1.5814 \times 10^5$	0.6679	$1.3424 \times 10^4$	0.3603

where  $E_{m_1}$  and  $E_{m_2}$  are the numerical solution errors for the grids containing  $m_1$  and  $m_2$  elements, respectively. The EOC and  $L^1$  and  $L^2$  errors of methane concentrations and cell-averaged pressures for the situation at time  $t = 0.48$  years are included in [Table 2](#) and [Table 3](#). EOC of concentrations in  $L^1$  norm are approximately 0.5, which is expected for the first order upwind FVM on hyperbolic problems with discontinuous solutions [17]. A comparison of the solutions on the individual grids using methane overall molar fractions at this time is depicted in [Fig. 4](#).

**Example 2.** In the next example, we simulate the methane injection into a vertical reservoir (i.e. with gravity) originally filled with propane. In [Fig. 5](#) isolines of methane overall molar fraction  $c_1 / (\sum_{i=1}^2 c_i)$  at different times are depicted. The value of molar fraction nearest to the injection corner is 0.95, and with each isoline towards the outflow corner the value decreases by 0.1. As in [Example 1](#), the fluid is in the single phase in the whole reservoir except for the mixing zone where the mixture occurs also in two phases as indicated by gray color. The computation to  $t = 1.14$  years lasted 13.2 hours. To validate our results, the problem was computed also by the *PT*-code. The obtained result at  $t = 1.14$  years is depicted in [Fig. 5\(d\)](#) (indication of the two-phase region was unavailable in the *PT*-code). The result differs slightly from ours in [Fig. 5\(c\)](#). The zone between 0.95 and 0.05 isoline is narrower in [Fig. 5\(d\)](#), however, we observed an incorrect pressure in the

**Table 3**

Experimental orders of convergence and errors of pressure  $p_K$  at time  $t = 0.48$  years for grids of  $m$  elements compared with the numerical solution on the grid of 8192 elements and the time step  $\Delta t = 195.3125$  s. On coarser grids,  $\Delta t \sim m^{-1}$ .

$m$	$\ E_m\ _1$	$EOC_1$	$\ E_m\ _2$	$EOC_2$
8	$3.0257 \times 10^8$	0.1283	$6.0661 \times 10^6$	0.1301
32	$2.7682 \times 10^8$	0.3544	$5.5430 \times 10^6$	0.3550
128	$2.1652 \times 10^8$	0.6859	$4.3339 \times 10^6$	0.6866
512	$1.3459 \times 10^8$	1.0166	$2.6928 \times 10^6$	1.0166
2048	$6.6528 \times 10^7$		$1.3310 \times 10^6$	

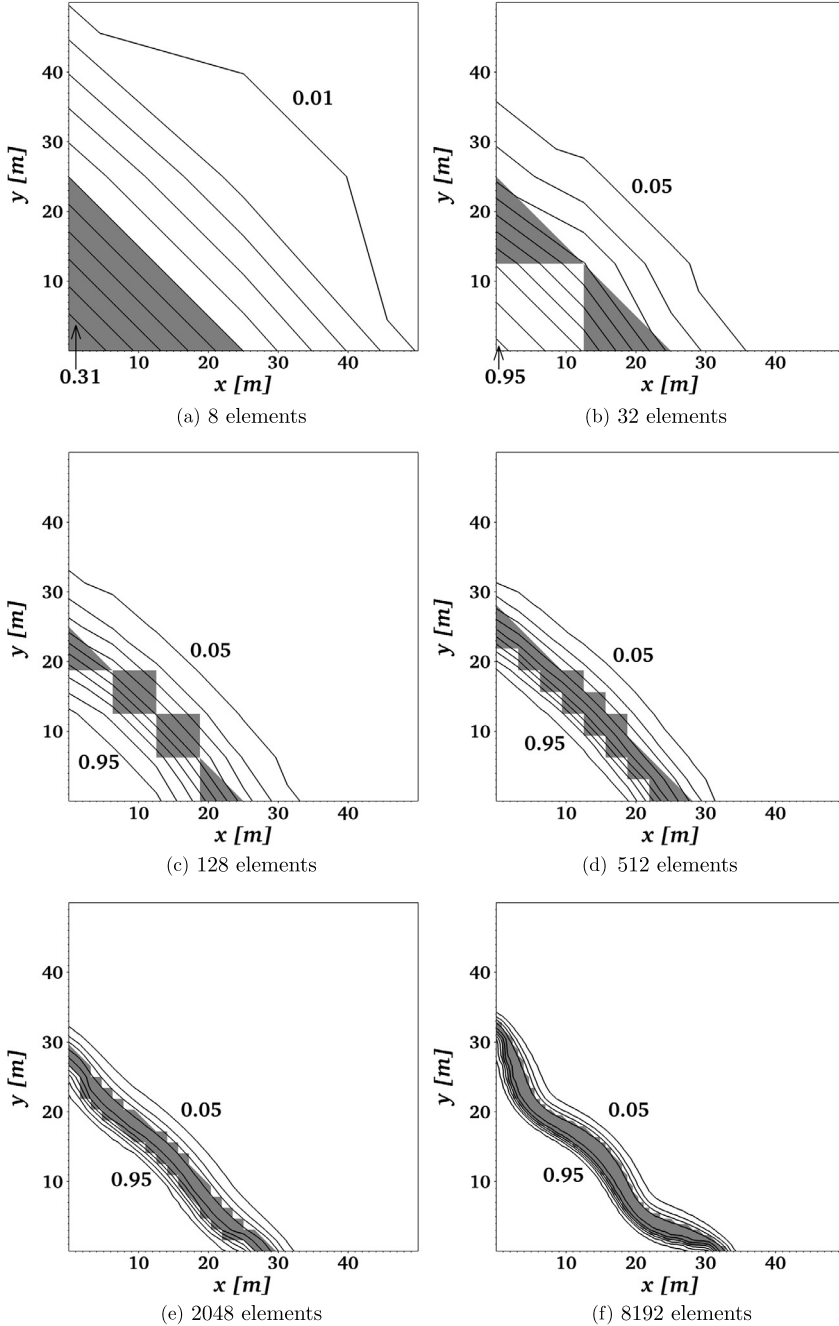


**Fig. 4.** Isolines of methane overall molar fraction and the two-phase region (gray color) computed on different grids at time  $t = 0.48$  years. Contours are distributed uniformly between the two printed values. Solutions are computed on the triangular grid: [Example 1](#).

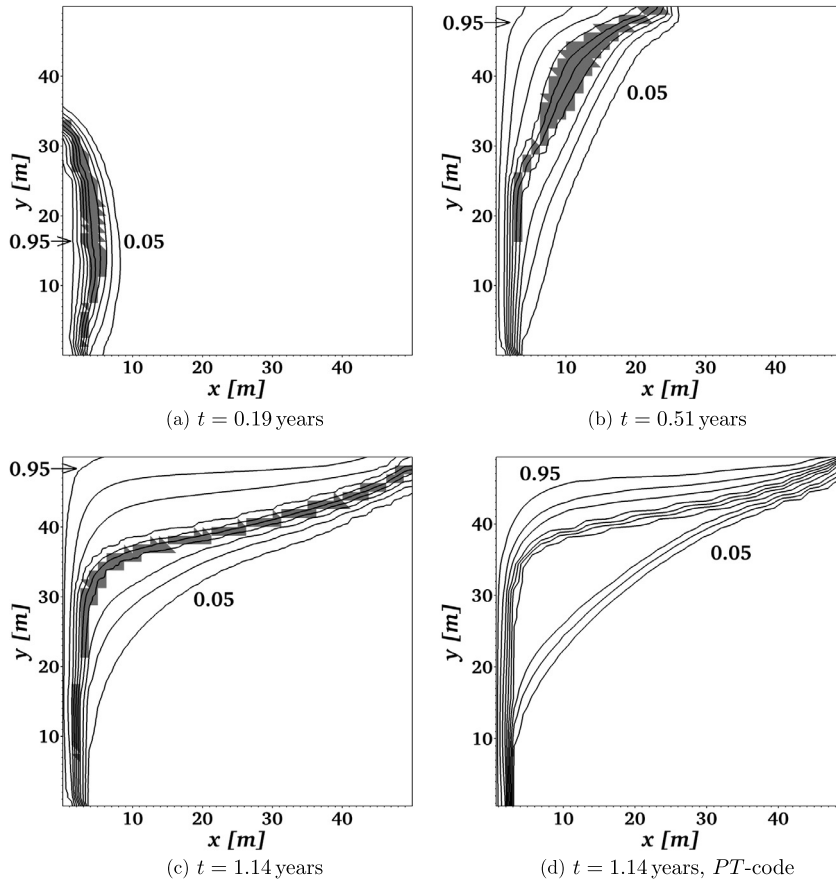


**Fig. 5.** Isolines of methane overall molar fraction and the two-phase region (gray color) at different times. Contours are distributed uniformly between the two printed values. The solution is computed on the triangular grid  $2 \times 40 \times 40$ ; (d) is computed on  $40 \times 40$  rectangles using the *PT*-code (the two-phase region is not indicated here); [Example 2](#).

**Table 4**

Relevant parameters of the Peng–Robinson equation of state (A.1) for [Examples 3, 4, and 8](#). Volume translation is not used.

$i$ (component)	$p_{ci}$ [MPa]	$T_{ci}$ [K]	$V_{ci}$ [ $\text{m}^3 \text{mol}^{-1}$ ]	$M_i$ [ $\text{g mol}^{-1}$ ]	$\omega_i$ [-]	$\delta_{i1}$ [-]	$\delta_{i2}$ [-]
1 ( $\text{CO}_2$ )	7.375	304.14	$9.416 \times 10^{-5}$	44	0.239	0	0.15
2 ( $\text{C}_3$ )	4.248	369.83	$2 \times 10^{-4}$	44.0962	0.153	0.15	0

outflowing element in the right upper corner of the domain in this result. Instead of a value close to 6.9 MPa (at the corner edges, there is prescribed exactly 6.9 MPa), which was observed in our result, there was 6.68 MPa in the result obtained by the *PT*-code. The lower pressure in the outflowing corner implies higher velocities, which can explain the difference in the molar fractions.

## 5.2. Injection of $\text{CO}_2$ into propane

Let us consider a cut through a propane reservoir at initial pressure  $p = 2.5$  MPa and temperature  $T = 311$  K. In the left bottom corner of the reservoir,  $\text{CO}_2$  is injected, and in the right upper corner, the mixture of  $\text{CO}_2$  and propane is produced ([Fig. 2\(b\)](#)). The injection rate of  $\text{CO}_2$  is  $42.5 \text{ m}^3/\text{day}$  at pressure 1 atm and temperature 293 K. The parameters of the Peng–Robinson equation of state for both components of the mixture are summarized in [Table 4](#). In these settings, the mixture can stay in the single phase or split into two phases. The boundary of the domain is impermeable except for the outflow corner where pressure  $p = 2.5$  MPa is maintained. Relative permeability depends linearly on saturation as  $k_{r\alpha}(S_\alpha) = S_\alpha$  for each phase  $\alpha$ .

**Example 3.** In [Fig. 6](#), a simulation of  $\text{CO}_2$  injection into a horizontal reservoir originally filled with propane is shown. Isolines of  $\text{CO}_2$  overall molar fraction  $c_1/(\sum_{i=1}^2 c_i)$  are distributed uniformly between the two displayed values of 0.95 and 0.05. The mixture stays in the single phase in the majority of the domain, only in the zone where the molar fractions are greater than

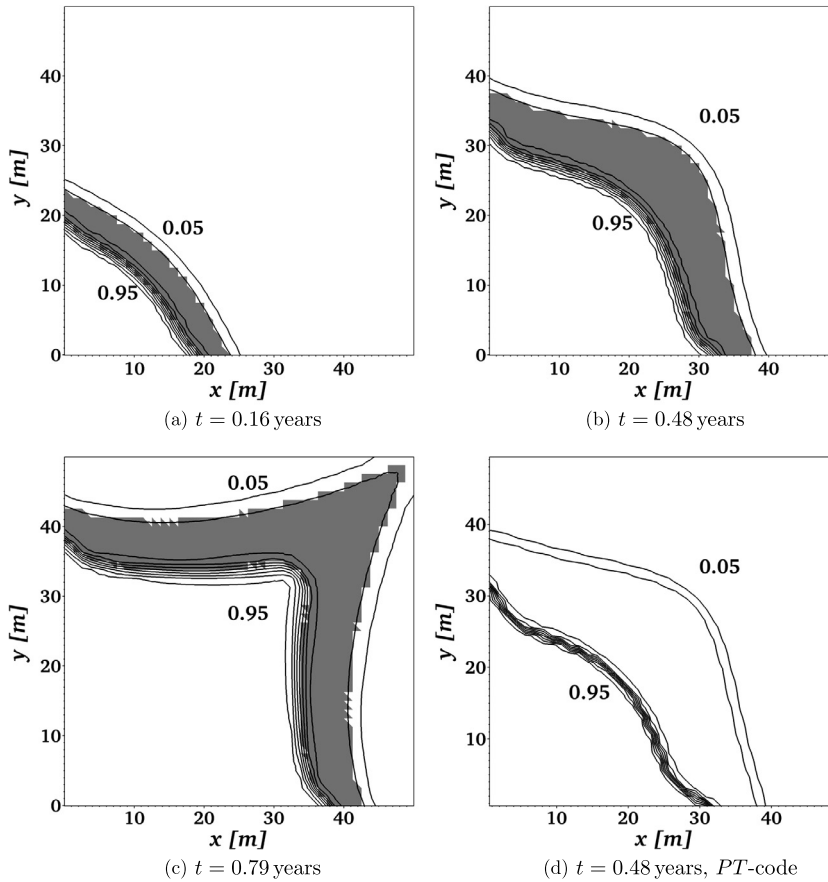


**Fig. 6.** Isolines of CO<sub>2</sub> overall molar fraction and the two-phase region (gray color) at different times. Contours are distributed uniformly between the two printed values. The solution is computed on the triangular grid  $2 \times 40 \times 40$ ; (d) is computed on  $40 \times 40$  rectangles using the *PT*-code (the two-phase region is not indicated here): [Example 3](#).

0.05 and less than 0.95, the two-phase region (colored in gray) appears. The computation to  $t = 0.79$  years lasted 6.4 hours. To validate our results, the problem was computed also by the *PT*-code. The zone between 0.95 and 0.05 isolines in the obtained result at  $t = 0.48$  years depicted in [Fig. 6\(d\)](#) (indication of the two-phase region was unavailable in the *PT*-code) is slightly wider than the one in [Fig. 6\(b\)](#) computed by our code.

**Example 4.** In this example, we simulate the CO<sub>2</sub> injection into a vertical propane reservoir. Uniformly distributed contours of CO<sub>2</sub> overall molar fractions  $c_1 / (\sum_{i=1}^2 c_i)$  between 0.95 and 0.05 are visualized in [Fig. 7](#). The single-phase mixture occupies a major part of the domain during the simulation but in the mixing zone a two-phase domain (gray color) also develops. At time  $t = 0.55$  years, we observed that there were the most two-phase elements of the whole simulation. Afterwards, the number of two-phase elements decreases. The computation to  $t = 0.79$  years lasted 8.8 hours. To validate our results, the problem was computed also by the *PT*-code. The obtained result at  $t = 0.48$  years is depicted in [Fig. 7\(d\)](#) (indication of the two-phase region was unavailable in the *PT*-code). The result differs from ours in [Fig. 7\(b\)](#), however, we observed an incorrect pressure in the outflowing element in the right upper corner of the domain in this result. Instead of a value close to 2.5 MPa (at the corner edges, there is prescribed exactly 2.5 MPa), which was observed in our result (2.51 MPa), there was 2.27 MPa in the other result. The lower pressure in the outflowing corner can cause different velocities, which explains the difference in the molar fractions. In the injection corner, the pressure was 2.53 MPa in the result obtained by the *PT*-code, while we observed 2.97 MPa in our result.

### 5.3. Injection of CO<sub>2</sub> into oil

In the third problem, let us consider a cut through an oil (8-component hydrocarbon mixture) reservoir at initial pressure  $p = 27.6$  MPa and temperature  $T = 403.15$  K. The initial overall molar fractions in the reservoir can be found in [Table 5](#). CO<sub>2</sub> is injected in one corner of the reservoir, and the mixture of CO<sub>2</sub> and oil is produced in the opposite corner. The injection rate of CO<sub>2</sub> is 133.33 m<sup>3</sup>/day at pressure 1 atm and temperature 293 K. The parameters of the Peng–Robinson equation of state for all components of the mixture are summarized in [Table 6](#). In these settings, the mixture can stay in the single

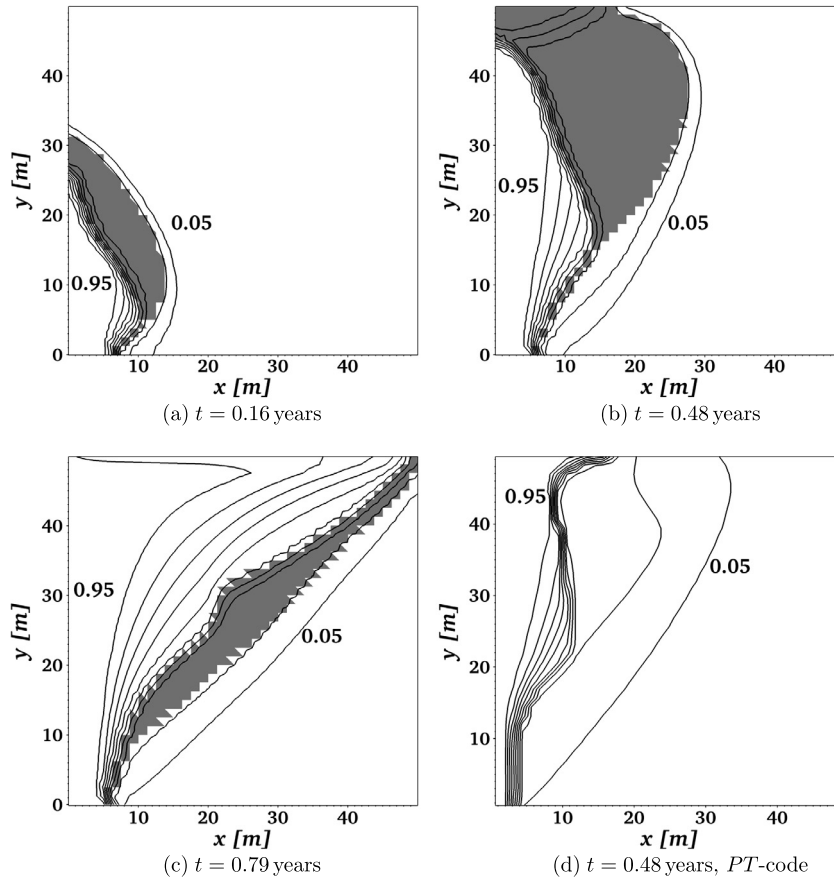


**Fig. 7.** Isolines of CO<sub>2</sub> overall molar fraction and the two-phase region (gray color) at different times. Contours are distributed uniformly between the two printed values. The solution is computed on the triangular grid  $2 \times 40 \times 40$ ; (d) is computed on  $40 \times 40$  rectangles using the *PT*-code (the two-phase region is not indicated here): [Example 4](#).

**Table 5**

The initial overall molar fractions in the reservoir.

Component	CO <sub>2</sub>	N <sub>2</sub>	C <sub>1</sub>	C <sub>2</sub> –C <sub>3</sub>	C <sub>4</sub> –C <sub>5</sub>	C <sub>6</sub> –C <sub>10</sub>	C <sub>11</sub> –C <sub>24</sub>	C <sub>25+</sub>
Overall molar fraction	0.0086	0.0028	0.4451	0.1207	0.0505	0.1328	0.1660	0.0735

**Table 6**

Relevant parameters of the Peng–Robinson equation of state (A.1) for [Examples 5, 6, and 7](#). Volume translation is not used.

$i$ (component)	$p_{ci}$ [MPa]	$T_{ci}$ [K]	$V_{ci}$ [m <sup>3</sup> mol <sup>-1</sup> ]	$M_i$ [g mol <sup>-1</sup> ]	$\omega_i$ [-]	$\delta_{i1}$ [-]	$\delta_{i2}$ [-]	$\delta_{i3}$ [-]	$\delta_{i4}$ [-]	$\delta_{i5}$ [-]	$\delta_{i6}$ [-]	$\delta_{i7}$ [-]	$\delta_{i8}$ [-]
1 (CO <sub>2</sub> )	7.375	304.14	$9.416 \times 10^{-5}$	44	0.239	0	0	0.15	0.15	0.15	0.15	0.15	0.08
2 (N <sub>2</sub> )	3.39	126.21	$8.988 \times 10^{-5}$	28	0.039	0	0	0.1	0.1	0.1	0.1	0.1	0.1
3 (C <sub>1</sub> )	4.599	190.56	$9.84 \times 10^{-5}$	16	0.011	0.15	0.1	0	0.0346	0.0392	0.0469	0.0635	0.1052
4 (C <sub>2</sub> –C <sub>3</sub> )	4.654	327.81	$1.6571 \times 10^{-4}$	34.96	0.11783	0.15	0.1	0.0346	0	0	0	0	0
5 (C <sub>4</sub> –C <sub>5</sub> )	3.609	435.62	$2.7522 \times 10^{-4}$	62.98	0.21032	0.15	0.1	0.0392	0	0	0	0	0
6 (C <sub>6</sub> –C <sub>10</sub> )	2.504	574.42	$4.6839 \times 10^{-4}$	110.21	0.41752	0.15	0.1	0.0469	0	0	0	0	0
7 (C <sub>11</sub> –C <sub>24</sub> )	1.502	708.95	$9.3876 \times 10^{-4}$	211.91	0.66317	0.15	0.1	0.0635	0	0	0	0	0
8 (C <sub>25+</sub> )	0.76	891.47	$1.9298 \times 10^{-3}$	462.79	1.7276	0.08	0.1	0.1052	0	0	0	0	0

phase or split into two phases. The boundary of the domain is impermeable except for the outflow corner where pressure  $p = 27.6$  MPa is maintained. Relative permeability depends quadratically on saturation as  $k_{r\alpha}(S_\alpha) = S_\alpha^2$  for each phase  $\alpha$ .

To validate our results, the following examples were computed also by the *PT*-code as in the previous simulations, but we have not included the results obtained by the *PT*-code for the sake of brevity.

**Example 5.** In [Fig. 9](#), a simulation of CO<sub>2</sub> injection in the left bottom corner of a horizontal reservoir originally filled with oil is shown. In the right upper corner, the mixture is produced. The reservoir is outlined in [Fig. 8\(a\)](#). In each of the 6

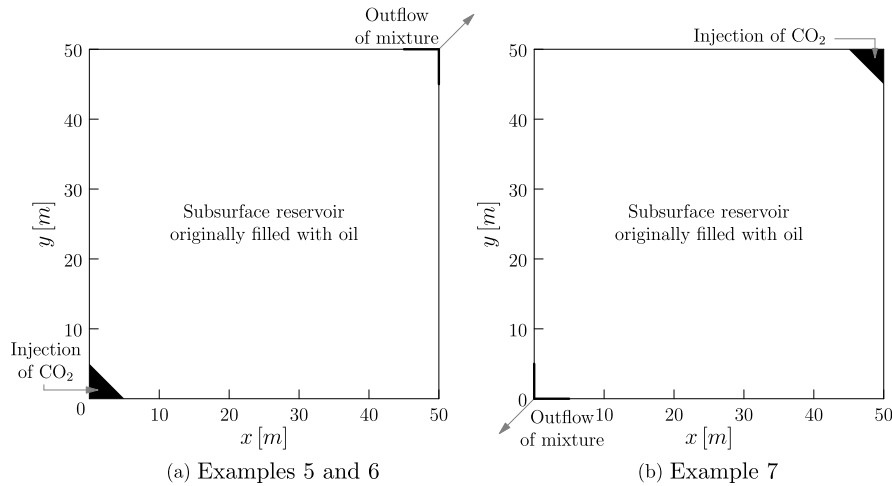


Fig. 8. Outlines of the simulated reservoirs for Examples 5–7.

plots, isolines of the overall molar fraction  $c_i / (\sum_{i=1}^8 c_i)$  are visualized for 1 of the 8 components at time  $t = 1.36$  years. Contours are distributed uniformly between the displayed values. In each figure the two-phase region is colored in gray color. In comparison with Examples 1–4, the two-phase region occupies a major part of the domain. The computation to  $t = 1.36$  years lasted 57.8 hours.

**Example 6.** This example is similar to Example 5, but this time we simulate injection of  $\text{CO}_2$  into a vertical oil reservoir.  $\text{CO}_2$  is injected in the left bottom corner and the mixture is produced in the right upper corner (as outlined in Fig. 8(a)). Results of the simulation at time  $t = 1.36$  years are shown in Fig. 10 using the isolines of the overall molar fractions  $c_i / (\sum_{i=1}^8 c_i)$  of 6 selected components, and the two-phase region is colored in gray. As in Example 5, also here, the two-phase region occupies a large part of the reservoir. The computation to  $t = 1.36$  years lasted 96.7 hours.

**Example 7.** In this example, we compute the injection of  $\text{CO}_2$  in the right upper corner of the vertical reservoir, whereas the mixture outflows in the left bottom corner (see Fig. 8(b)). Fig. 11 shows results of the simulation at time  $t = 1.36$  years. Isolines of the overall molar fraction  $c_i / (\sum_{i=1}^8 c_i)$  are visualized for the same components as in Examples 5 and 6. Again, the gray-colored two-phase region is spread over a significant part of the reservoir. The computation to  $t = 1.36$  years lasted 75.3 hours.

#### 5.4. $\text{CO}_2$ close to the saturation pressure

**Example 8.** In the last example, we simulate an isothermal injection of  $\text{CO}_2$  into a reservoir that is filled with pure gas  $\text{CO}_2$  at temperature  $T = 280$  K and  $p = 4$  MPa. Note that the saturated vapor pressure of  $\text{CO}_2$  at 280 K is 4.13 MPa.  $\text{CO}_2$  is injected in the left bottom corner of the reservoir and produced in the right upper corner. The injection rate is  $42.5 \text{ m}^3/\text{day}$  at pressure 1 atm and temperature 293 K. The parameters of the Peng–Robinson equation of state for  $\text{CO}_2$  are summarized in Table 4 (first line). The medium has a low permeability  $\mathbf{K} = k = 9.87 \times 10^{-17} \text{ m}^2$  (i.e. 0.1 mD) and porosity  $\phi = 0.2$ . The boundary of the domain is impermeable except for the outflow corner where pressure  $p = 4$  MPa is maintained. Relative permeability depends linearly on saturation as  $k_{r\alpha}(S_\alpha) = S_\alpha$  for each phase  $\alpha$ .

Due to the injection, the pressure in the vicinity of the injection point rises above the value of the saturation pressure and the liquid  $\text{CO}_2$  phase should appear. Fig. 12 shows the result of our code at four different times. The computation to  $t = 10.14$  years lasted 4.6 hours. The liquid  $\text{CO}_2$  with density approximately  $873 \text{ kg m}^{-3}$  displaces the vapor with density approximately  $118 \text{ kg m}^{-3}$ . The two-phase elements (gray) correspond well with the dashed isoline of the saturation pressure (see Fig. 12). The  $PT$ -code (based on [13,14,24]) used for this simulation crashes due to the problem with the phase identification. This problem shows the advantages of the  $VT$ -based formulation which does not require the phase identification.

## 6. Summary and conclusions

We have developed a new formulation of the compositional model for the reservoir simulation. The new feature of the model is that it uses computation of phase equilibria at constant temperature and volume rather than pressure. Compared to the traditional  $PT$ -based formulation, the new formulation in terms of  $VT$  is not only more robust, but also provides a convenient and natural way for the pressure computation. In the new formulation, the equation of state does not have to be

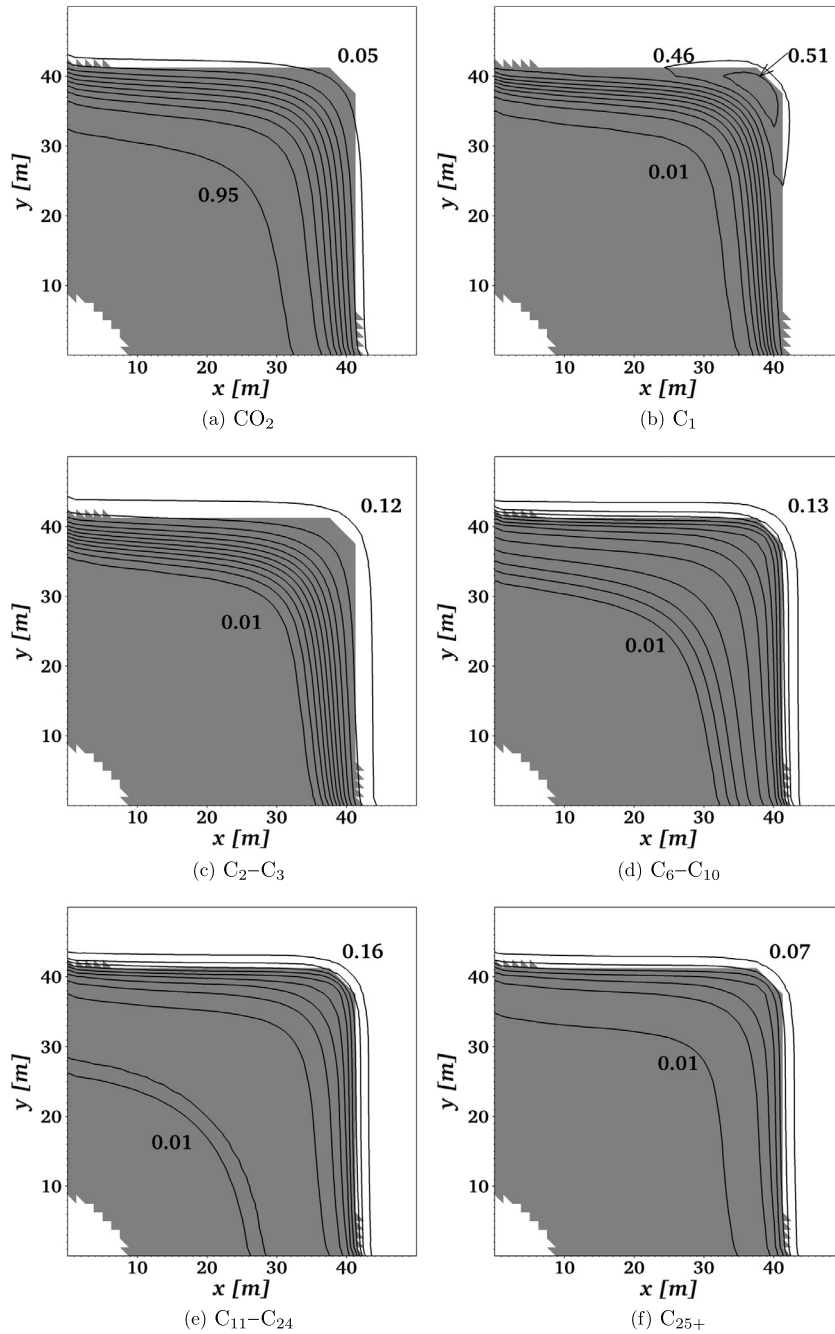


**Fig. 9.** Isolines of the overall molar fractions and the two-phase region (gray color) at  $t = 1.36$  years. Contours are distributed uniformly between the two printed values. The solution is computed on the triangular grid  $2 \times 40 \times 40$ : [Example 5](#).

inverted, and thus the root selection problem does not appear. We have tested the model on eight examples involving binary and multicomponent mixtures described by the Peng–Robinson equation of state. We expect that the same approach can be used for other pressure-explicit equations of state as well. Moreover, we expect that the advantage of the fact that there is no need for inversion in the equation of state will appear to be beneficial for simulations using non-cubic equations of state. These equations of state can describe correctly association in the mixtures involving polar components (e.g.  $\text{CO}_2 + \text{H}_2\text{O}$ ) and, thus, have important applications in problems related to carbon sequestration [18,16]. Extension of our approach to these equations of state is a subject of current research.

We have discretized the model using a combination of the MHFEM and FVM for the computation of two-phase compressible flow of a mixture in porous media in 2D. In comparison with the traditional approaches, our approximation of the component flux between elements does not depend on the phase identification and pairing of phases between elements.

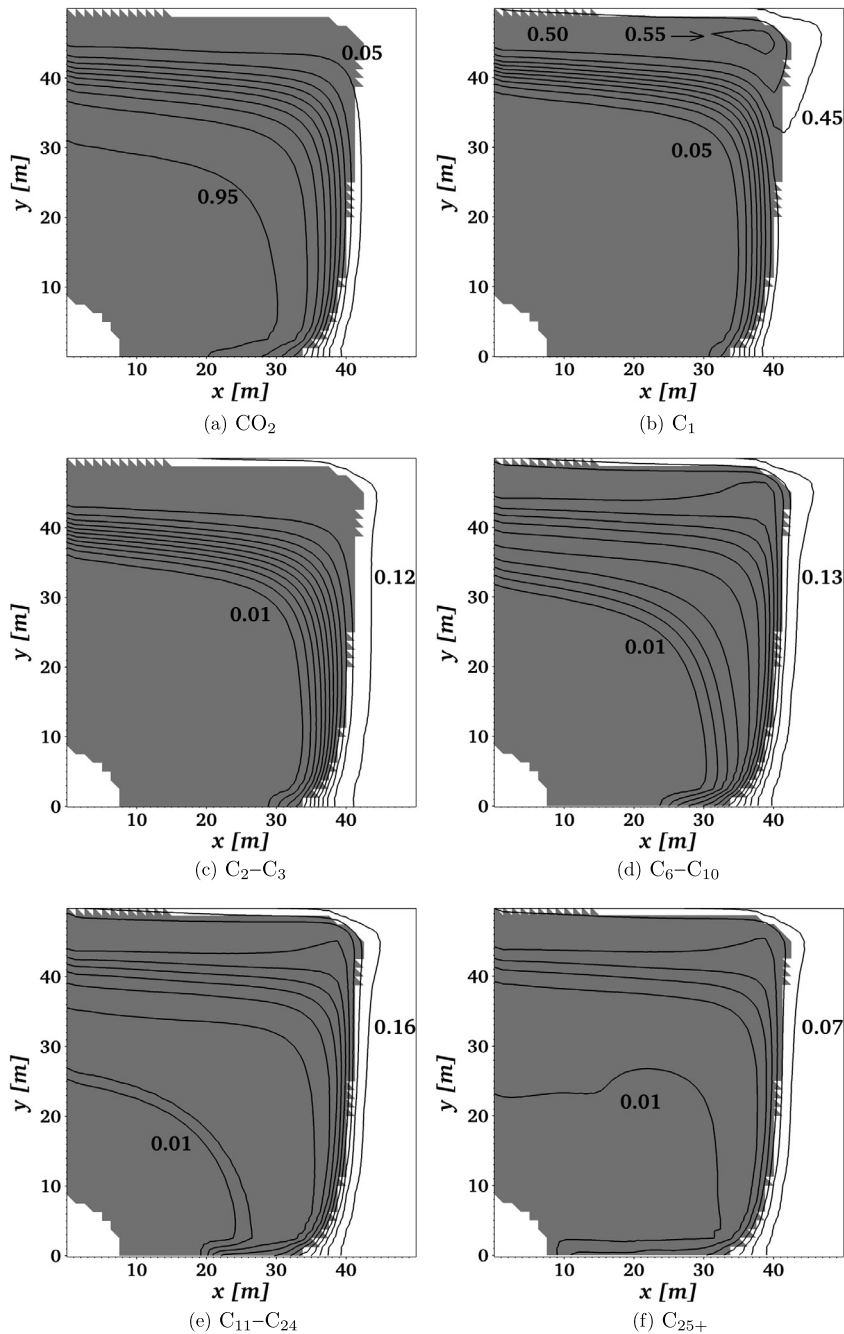


**Fig. 10.** Isolines of the overall molar fractions and the two-phase region (gray color) at  $t = 1.36$  years. Contours are distributed uniformly between the two printed values. The solution is computed on the triangular grid  $2 \times 40 \times 40$ : [Example 6](#).

This feature of the model will be also advantageous in problems related to carbon sequestration as typically  $\text{CO}_2$  is injected into the reservoir in the supercritical state.

Our method is fully coupled, fully implicit and is therefore much more expensive in comparison with the decoupled (sequential) IMPEC approaches. In this work, we focused on the robustness of the formulation rather than the CPU costs. We believe that the robustness of the  $VT$ -flash and flux evaluation which does not depend on the phase identification can be exploited also in the sequential schemes. Development of such schemes is another subject of our current research.

Many questions related to the new formulation remain open, e.g. how to include diffusion or capillarity in the  $VT$ -based model. For example, capillarity in the compositional simulation has traditionally been formulated using the extension of the concepts developed in the immiscible flow. Here, the  $VT$ -based formulation seems to be of great advantage with respect to  $PT$ , but currently available theories of capillarity rely heavily on the phase identification. We believe that the model

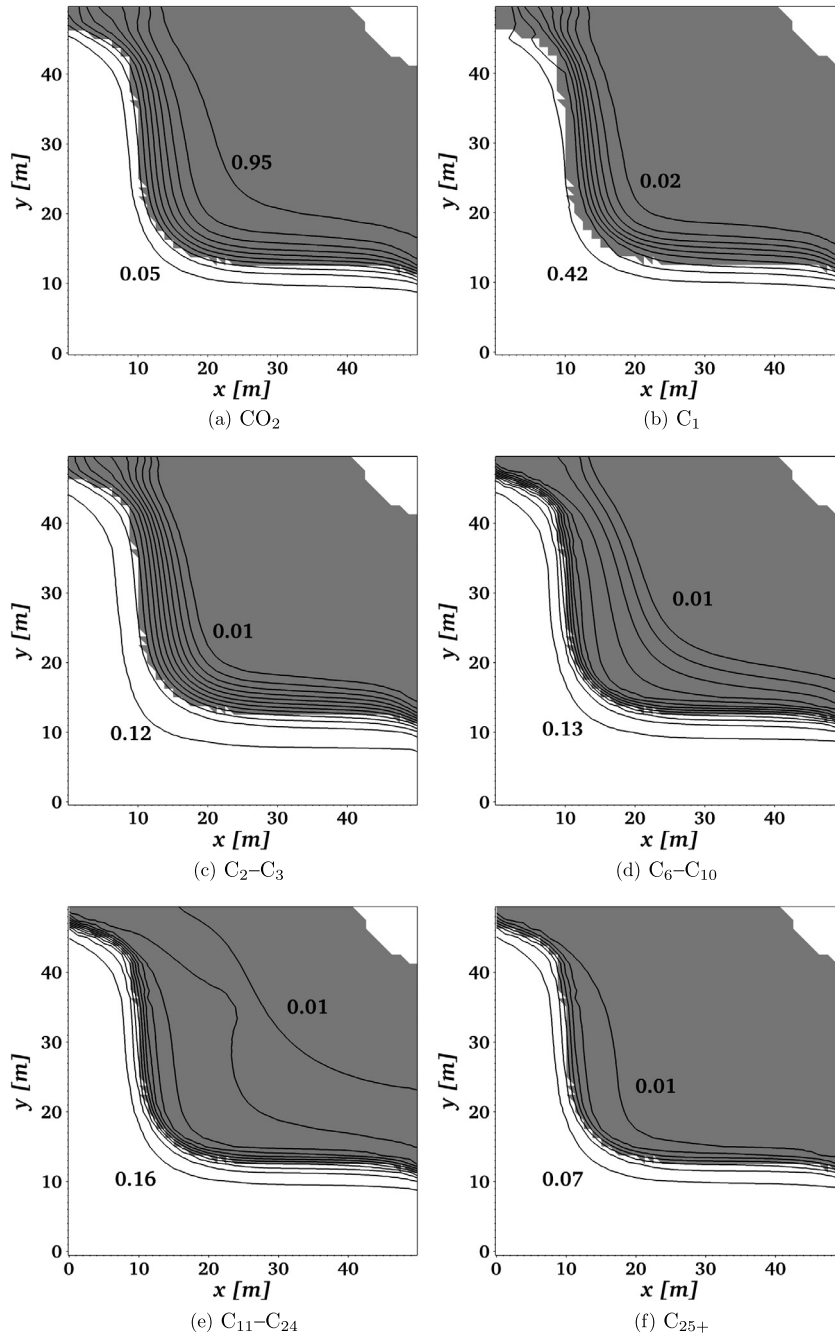


**Fig. 11.** Isolines of the overall molar fractions and the two-phase region (gray color) at  $t = 1.36$  years. Contours are distributed uniformly between the two printed values. The solution is computed on the triangular grid  $2 \times 40 \times 40$ : [Example 7](#).

concept proposed in this paper can be extended to include capillarity and diffusion, although this may require a non-trivial revision of basic concepts and the way we usually describe these phenomena. Development of such extensions is subject of our future research.

### Acknowledgements

This work has been supported by the project P105/11/1507 Development of Computational Models for Simulation of CO<sub>2</sub> Sequestration of the Czech Science Foundation and by the project KONTAKT II LH 12064 Computational Methods in Thermodynamics of Hydrocarbon Mixtures of the Ministry of Education, Youth and Sport of the Czech Republic.

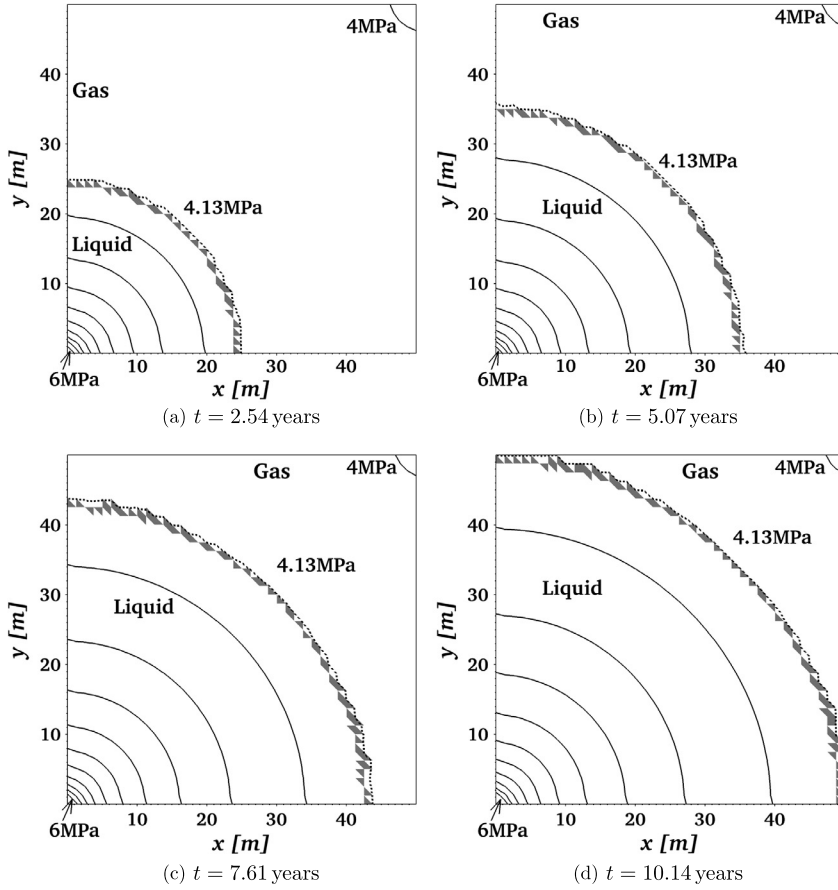


**Fig. 12.** Isolines of the cell-averaged pressure  $p_K$  and the two-phase elements (gray color) at different times. Solid contours are distributed uniformly between the two printed values. Dashed contours represent the saturation pressure and separates the liquid and gas zones. The solution is computed on the triangular grid  $2 \times 40 \times 40$ : Example 8.

## Appendix A. Details of the constitutive relations

Pressure in (6b) is given by the Peng–Robinson equation of state [30,12,26,27] as

$$p(T, c_1, \dots, c_{n_c}) = \frac{RT \sum_{i=1}^{n_c} c_i}{1 - \sum_{i=1}^{n_c} b_i c_i} - \frac{\sum_{i=1}^{n_c} \sum_{j=1}^{n_c} a_{ij} c_i c_j}{1 + 2 \sum_{i=1}^{n_c} b_i c_i - (\sum_{i=1}^{n_c} b_i c_i)^2}. \quad (\text{A.1})$$

In Eq. (A.1),  $R = 8.314472 \text{ JK}^{-1} \text{ mol}^{-1}$  is the universal gas constant and

$$a_{ij} = (1 - \delta_{ij}) \sqrt{a_i a_j}, \quad a_i = 0.45724 \frac{R^2 T_{ci}^2}{p_{ci}} [1 + m_i (1 - \sqrt{T_{ri}})]^2, \\ m_i = \begin{cases} 0.37464 + 1.54226 \omega_i - 0.26992 \omega_i^2 & \text{for } \omega_i < 0.5, \\ 0.3796 + 1.485 \omega_i - 0.1644 \omega_i^2 + 0.01667 \omega_i^3 & \text{for } \omega_i \geq 0.5, \end{cases} \\ T_{ri} = \frac{T}{T_{ci}}, \quad b_i = 0.0778 \frac{RT_{ci}}{p_{ci}}, \quad (\text{A.2})$$

where  $\delta_{ij}$  is the binary interaction coefficient [-];  $T_{ci}$ ,  $p_{ci}$ ,  $\omega_i$ ,  $T_{ri}$  are the critical temperature [K], critical pressure [Pa], acentric factor [-], reduced temperature [-], respectively – all corresponding to the  $i$ -th component.

The condition of chemical equilibrium (6c) can be rewritten in terms of the volume function coefficients, which were introduced in [26] to replace fugacities in the VT-based formulations. The equivalent condition to (6c) reads as

$$\frac{c_{\alpha,i}}{\varphi_i(T, c_{\alpha,1}, \dots, c_{\alpha,n_c})} = \frac{c_{\beta,i}}{\varphi_i(T, c_{\beta,1}, \dots, c_{\beta,n_c})}, \quad \forall \alpha \neq \beta, \quad \forall i = 1, \dots, n_c, \quad (\text{A.3})$$

where the volume function coefficient  $\varphi_i$  for the Peng–Robinson equation of state reads as

$$\begin{aligned} & \ln \varphi_i(T, c_1, \dots, c_{n_c}) \\ &= \ln \left( 1 - \sum_{j=1}^{n_c} b_j c_j \right) - \frac{b_i \sum_{j=1}^{n_c} c_j}{1 - \sum_{j=1}^{n_c} b_j c_j} + \frac{b_i \sum_{j=1}^{n_c} \sum_{k=1}^{n_c} a_{jk} c_j c_k}{RT \sum_{j=1}^{n_c} b_j c_j (1 + 2 \sum_{j=1}^{n_c} b_j c_j - (\sum_{j=1}^{n_c} b_j c_j)^2)} \\ & - \frac{1}{\sqrt{2} RT \sum_{j=1}^{n_c} b_j c_j} \left( \frac{b_i \sum_{j=1}^{n_c} \sum_{k=1}^{n_c} a_{jk} c_j c_k}{2 \sum_{j=1}^{n_c} b_j c_j} - \sum_{j=1}^{n_c} a_{ij} c_j \right) \ln \left| \frac{1 + (1 + \sqrt{2}) \sum_{j=1}^{n_c} b_j c_j}{1 + (1 - \sqrt{2}) \sum_{j=1}^{n_c} b_j c_j} \right|. \end{aligned} \tag{A.4}$$

Details of the definition and basic properties of the volume functions and volume function coefficients as well as derivation of the last formula can be found in [26].

**Appendix B. Raviart–Thomas basis functions and details of the MHFEM**

In this part, we describe details of derivation of discrete Darcy’s law (19) using the Raviart–Thomas space [3,4,31,24]. The Raviart–Thomas space of the lowest order  $RT_0(K)$ , over an element  $K$  from a triangulation  $\mathcal{T}_\Omega$  (consisting of triangles) of the domain  $\Omega$ , is generated by the basis functions

$$\mathbf{w}_{K,E}(\mathbf{x}) = \frac{1}{2|K|}(\mathbf{x} - \mathbf{N}_{K,E}), \quad \forall \mathbf{x} \in K, \quad E \in \partial K, \tag{B.1}$$

where  $\mathbf{N}_{K,E} \in K$  is a node against edge  $E$ . The basis functions (B.1) satisfy the following properties

$$\nabla \cdot \mathbf{w}_{K,E}(\mathbf{x}) = \frac{1}{|K|}, \quad \mathbf{w}_{K,E}(\mathbf{x}) \cdot \mathbf{n}_{K,E'} = \frac{\delta_{E,E'}}{|E|}. \tag{B.2}$$

Multiplying (12) with the basis function  $\mathbf{w}_{K,E}$ , and integrating over element  $K$ , we can write

$$\int_K \nabla p \cdot \mathbf{w}_{K,E'} = - \left( \sum_{\alpha \in \Pi(K)} c_{\alpha,K} \lambda_{\alpha,K} \right)^{-1} \sum_{E \in \partial K} q_{K,E} \int_K \mathbf{K}^{-1} \mathbf{w}_{K,E} \cdot \mathbf{w}_{K,E'} + \tilde{Q}_K \int_K \mathbf{g} \cdot \mathbf{w}_{K,E'}, \tag{B.3}$$

where we have used (18), the mean value theorem, and  $\Pi(K)$  denotes all phases on element  $K$ . On the other hand, using the Green theorem, the mean value theorem, and properties (B.2), we obtain

$$\int_K \nabla p \cdot \mathbf{w}_{K,E'} = \sum_{E \in \partial K} \int_E p \mathbf{w}_{K,E'} \cdot \mathbf{n}_{K,E} - \int_K p \nabla \cdot \mathbf{w}_{K,E'} = \frac{1}{|E'|} \int_{E'} p - \frac{1}{|K|} \int_K p. \tag{B.4}$$

Denoting

$$\begin{aligned} A_{K,E,E'} &= \int_K \mathbf{K}^{-1} \mathbf{w}_{K,E} \cdot \mathbf{w}_{K,E'}, & G_{K,E'} &= \int_K \mathbf{g} \cdot \mathbf{w}_{K,E'}, \\ \hat{p}_{K,E'} &= \frac{1}{|E'|} \int_{E'} p, & p_K &= \frac{1}{|K|} \int_K p, \end{aligned} \tag{B.5}$$

we combine (B.3) and (B.4) into

$$\left( \sum_{\alpha \in \Pi(K)} c_{\alpha,K} \lambda_{\alpha,K} \right)^{-1} \sum_{E \in \partial K} q_{K,E} A_{K,E,E'} = p_K - \hat{p}_{K,E'} + \tilde{Q}_K G_{K,E'}. \tag{B.6}$$

Assuming that  $\mathbf{K}$  is a uniformly positive-definite tensor (see [20]), i.e.

$$\exists \alpha_0 > 0: \quad \alpha_0 \sum_{i=1}^d \xi_i^2 \leq \sum_{i,j=1}^d [\mathbf{K}(\mathbf{x})]_{i,j} \xi_i \xi_j, \quad \forall \boldsymbol{\xi} \in \mathbb{R}^d, \tag{B.7}$$

for almost all  $\mathbf{x} \in \Omega$ , it is possible to invert the matrix  $\mathbf{A}_K = (A_{K,E,E'})_{E,E' \in \partial K}$ . Multiplying (B.6) in a vector form by  $\mathbf{A}_K^{-1}$ , we obtain for  $K \in \mathcal{T}_\Omega$  and  $E \in \partial K$

$$q_{K,E} = \sum_{\alpha \in \Pi(K)} c_{\alpha,K} \lambda_{\alpha,K} \left( \alpha_E^K p_K - \sum_{E' \in \partial K} \beta_{E,E'}^K \widehat{p}_{K,E'} + \gamma_E^K \widetilde{Q}_K \right), \quad (\text{B.8})$$

which is Darcy's law (19) with coefficients  $\alpha_E^K$ ,  $\beta_{E,E'}^K$ , and  $\gamma_E^K$  given by

$$\alpha_E^K = \sum_{E' \in \partial K} A_{K,E,E'}^{-1}, \quad \beta_{E,E'}^K = A_{K,E,E'}^{-1}, \quad \gamma_E^K = \sum_{E' \in \partial K} A_{K,E,E'}^{-1} G_{K,E'}, \quad (\text{B.9})$$

where  $A_{K,E,E'}^{-1}$  is the element of the inverse matrix  $\mathbf{A}_K^{-1}$ .

## References

- [1] G. Ács, S. Doleschall, É. Farkas, General purpose compositional model, *SPE J.* 25 (4) (1985) 543–553 (SPE-10515-PA).
- [2] A. Bourgeat, M. Jurak, F. Smaï, On persistent primary variables for numerical modeling of gas migration in a nuclear waste repository, *Comput. Geosci.* 17 (2) (2013) 287–305.
- [3] F. Brezzi, M. Fortin, *Mixed and Hybrid Finite Element Methods*, Springer-Verlag, New York Inc., 1991.
- [4] G. Chavent, J.E. Roberts, A unified physical presentation of mixed, mixed-hybrid finite elements and standard finite difference approximations for the determination of velocities in waterflow problems, *Adv. Water Resour.* 14 (6) (1991) 329–348.
- [5] Z. Chen, G. Huan, Y. Ma, *Computational Methods for Multiphase Flows in Porous Media*, SIAM, Philadelphia, 2006.
- [6] H. Class, R. Helmig, P. Bastian, Numerical simulation of non-isothermal multiphase multicomponent processes in porous media. 1. An efficient solution technique, *Adv. Water Resour.* 25 (5) (2002) 533–550.
- [7] T.A. Davis, A column pre-ordering strategy for the unsymmetric-pattern multifrontal method, *ACM Trans. Math. Softw.* 30 (2) (2004) 165–195.
- [8] T.A. Davis, Algorithm 832: UMFPACK, an unsymmetric-pattern multifrontal method, *ACM Trans. Math. Softw.* 30 (2) (2004) 196–199.
- [9] T.A. Davis, I.S. Duff, A combined unifrontal/multifrontal method for unsymmetric sparse matrices, *ACM Trans. Math. Softw.* 25 (1) (1999) 1–19.
- [10] T.A. Davis, I.S. Duff, An unsymmetric-pattern multifrontal method for sparse LU factorization, *SIAM J. Matrix Anal. Appl.* 18 (1) (1997) 140–158.
- [11] M. Delshad, S.G. Thomas, M.F. Wheeler, Parallel numerical reservoir simulations of nonisothermal compositional flow and chemistry, *SPE J.* 16 (2) (2011) 239–248.
- [12] A. Firoozabadi, *Thermodynamics of Hydrocarbon Reservoirs*, McGraw-Hill, NY, 1998.
- [13] H. Hoteit, A. Firoozabadi, Multicomponent fluid flow by discontinuous Galerkin and mixed methods in unfractured and fractured media, *Water Resour. Res.* 41 (2005), <http://dx.doi.org/10.1029/2005WR004339>, W11412.
- [14] H. Hoteit, A. Firoozabadi, Compositional modeling by the combined discontinuous Galerkin and mixed methods, *SPE J.* (March 2006) 19–34.
- [15] T. Jindrová, Computational methods in thermodynamics of multicomponent mixtures, Master thesis, Department of Mathematics, Faculty of Nuclear Sciences and Physical Engineering, Czech Technical University in Prague, 2013.
- [16] T. Jindrová, J. Mikyška, Fast and robust algorithm for calculation of two-phase equilibria at given volume, temperature, and moles, *Fluid Phase Equilib.* 353 (2013) 101–114.
- [17] R.J. Leveque, *Finite Volume Methods for Hyperbolic Problems*, Cambridge University Press, Cambridge, 2002.
- [18] Z. Li, A. Firoozabadi, Cubic-plus-association equation of state for water-containing mixtures: is “cross association” Necessary? *AIChE J.* 56 (7) (2009) 1803–1813.
- [19] J. Lohrenz, B.G. Bray, C.R. Clark, Calculating viscosities of reservoir fluids from their compositions, *J. Pet. Technol.* (Oct. 1964) 1171–1176.
- [20] J. Maryška, M. Rozložník, M. Tůma, Mixed-hybrid finite element approximation of the potential fluid flow problem, *J. Comput. Appl. Math.* 63 (1995) 383–392.
- [21] M.L. Michelsen, The isothermal flash problem. 1. Stability, *Fluid Phase Equilib.* 9 (1) (1982) 1–19.
- [22] M.L. Michelsen, The isothermal flash problem. 2. Phase split calculation, *Fluid Phase Equilib.* 9 (1) (1982) 21–40.
- [23] M.L. Michelsen, J.M. Mollerup, *Thermodynamic Models: Fundamentals and Computational Aspects*, Tie-Line Publications, 2004.
- [24] J. Mikyška, A. Firoozabadi, Implementation of higher-order methods for robust and efficient compositional simulation, *J. Comput. Phys.* 229 (2010) 2898–2913.
- [25] J. Mikyška, A. Firoozabadi, Application of high-resolution methods in compositional simulations, *Proc. Comput. Sci.* 4 (2011) 928–937.
- [26] J. Mikyška, A. Firoozabadi, A new thermodynamic function for phase-splitting at constant temperature, moles, and volume, *AIChE J.* 57 (7) (2011) 1897–1904.
- [27] J. Mikyška, A. Firoozabadi, Investigation of mixture stability at given volume, temperature, and number of moles, *Fluid Phase Equilib.* 321 (2012) 1–9.
- [28] J. Moortgat, S. Sun, A. Firoozabadi, Compositional modeling of three-phase flow with gravity using higher-order finite element methods, *Water Resour. Res.* 47 (2011), <http://dx.doi.org/10.1029/2010WR009801>, W05511.
- [29] R. Neumann, P. Bastian, O. Ippisch, Modeling and simulation of two-phase two-component flow with disappearing nonwetting phase, *Comput. Geosci.* 17 (2013) 139–149.
- [30] D.Y. Peng, D.B. Robinson, A new two-constant equation of state, *Ind. Eng. Chem. Fundam.* 15 (1976) 59–64.
- [31] O. Polívka, J. Mikyška, Numerical simulation of multicomponent compressible flow in porous medium, *J. Math. Ind.* 3 (2011) 53–60, JMI2011C-7.
- [32] O. Polívka, J. Mikyška, Combined mixed-hybrid finite element-finite volume scheme for computation of multicomponent compressible flow in porous media, in: *Numerical Mathematics and Advanced Applications 2011*, Proceedings of ENUMATH 2011, Springer-Verlag, Berlin, Heidelberg, 2013, pp. 559–567.
- [33] A. Quarteroni, R. Sacco, F. Saleri, *Numerical Mathematics*, Springer-Verlag, New York, 2000.
- [34] S. Sun, A. Firoozabadi, J. Kou, Numerical modeling of two-phase binary fluid mixing using mixed finite elements, *Comput. Geosci.* 16 (4) (2012) 1101–1124.
- [35] L.C. Young, R.E. Stephenson, A generalized compositional approach for reservoir simulation, *SPE J.* 23 (5) (1983) 727–742.